



Titania/reduced graphene oxide nanocomposites (TiO₂/rGO) as an efficient photocatalyst for the effective degradation of brilliant green in aqueous media: effect of peroxymonosulfate and operational parameters

Qaiser Khan¹ · Murtaza Sayed¹ · Ikhtiar Gul¹

Received: 17 October 2022 / Accepted: 24 April 2023 / Published online: 9 May 2023
© The Author(s), under exclusive licence to Springer-Verlag GmbH Germany, part of Springer Nature 2023

Abstract

This study is focused on synthesis of highly efficient Titania/reduced Graphene Oxide (TiO₂/rGO) nanocomposites by means of simple hydrothermal technique. The TiO₂/rGO were synthesized in different ratios of 0.5, 1.0, 2.0, and 3% by varying the concentration of rGO while the concentration of TiO₂ was kept constant and the obtained samples were designated as TrG0.5, TrG1, TrG2, and TrG3 respectively. Different characterization techniques (SEM, TEM, HRTEM, XRD, EDX, TGA, UV-DRS, PL, EIS, and BET) showed high crystallinity, small crystallite size (18.4 nm), high thermal stability, high purity, low band gap energy ($E_g = 3.12$ eV), and high surface area (65.989 m²/g) for the as-synthesized TiO₂/rGO nanocomposite. The efficiencies of TiO₂/rGO were determined in terms of brilliant green (BG) dye degradation in aqueous media under UV light. The results revealed that 2% TiO₂/rGO (TrG2) showed high efficiency for BG degradation with the k_{app} of 0.023 min⁻¹ compared to TiO₂ alone (k_{app} of 0.006 min⁻¹). The rate of BG degradation was further synergised by the addition of peroxymonosulfate (PMS) to the system. The degradation of BG was improved to 99.4% by the incorporation of PMS in aqueous media compared to TrG2 alone. Furthermore, the degradation of BG was also examined in various media (neutral, acidic, and basic). The results revealed that by increasing pH of the medium from 3.85 to 8.2 the degradation of BG was enhanced from 99.4 to 99.9% with the corresponding k_{app} of 0.0602 min⁻¹. Moreover, the photocatalytic degradation of BG followed the *pseudo-first-order* kinetics. Radical scavenging experiments showed that $\bullet\text{OH}$ and $\text{SO}_4^{\bullet-}$ were the main species responsible for the degradation of BG under UV light. Besides, for determining the efficiency of as-synthesized TrG2/PMS system, the degradation of BG was also performed in various water types (distilled water, tap water, synthetic wastewater, and industrial wastewater). The degradation products (DPs) of BG and their corresponding pathways were proposed, accordingly.

Keywords Wastewater · Contaminants · Advanced oxidation processes (AOPs) · Photocatalysis · Titania/reduced graphene oxide nanocomposites · (TiO₂/rGO) · Peroxymonosulfate (PMS) · Brilliant green · Dyes · Degradation

Introduction

Advanced oxidation processes produce highly reactive hydroxyl radical specie ($\bullet\text{OH}$) that readily attack on the contaminant and cause its degradation in wastewater (S.

Khan et al. 2019). Hydroxyl radicals strike the contaminants non-selectively and rapidly. Because $\bullet\text{OH}$ can be produced in a variety of methods, these techniques can be classified as multifunctional technologies. AOPs are considered more effective tool that cause the degradation of highly hazardous organic contaminants releasing from various industries including pharmaceutical, textiles, and dye industries, etc. Some of these processes work on pure light (sun light) instead of using synthetic light resources i.e., Ultraviolet, Visible, Mercury light etc. Although advanced oxidation methods employ a variety of reactive systems, they are all characterized by the formation of $\bullet\text{OH}$ as a chemical characteristic. $\bullet\text{OH}$, is a highly reactive specie that attacks

Responsible Editor: Sami Rtimi

✉ Murtaza Sayed
murtazasayed@uop.edu.pk

¹ Radiation and Environmental Chemistry lab, National Centre of Excellence in Physical Chemistry, University of Peshawar, Peshawar, Pakistan

the majority of contaminants present in aqueous media with rate constant ($k_{app} = 10^6\text{--}10^9 \text{ M}^{-1} \text{ sec}^{-1}$) (Ameta et al. 2018; Arslan et al. 1999; Wang and Xu 2012). These radicals attack the contaminants non-selectivity, which is a desirable feature for a specie employed in the treatment of wastewater and pollution control, particularly for the breakdown of pollutants in aqueous media (Abdel Rahman and Hung 2020; Jian et al. 2021; Trojanowicz et al. 2018; Yu et al. 2021). Besides $\bullet\text{OH}$, the sulfate radical ($\text{SO}_4\bullet^-$)-based advanced oxidation techniques are most widely used nowadays. Due to the high selective nature of $\text{SO}_4\bullet^-$ it readily attack on the contaminants and cause its effective degradations. Peroxymonosulfate (PMS) and persulfate (PS) are the most common oxidizing agents employed for the generation of $\text{SO}_4\bullet^-$. These oxidants may get activated by different methods (heat, light, and transitions metals) to produce the $\text{SO}_4\bullet^-$ (Khan et al. 2017).

Nowadays, the TiO_2 based photocatalysis is considered one of the efficient technique for the degradation of contaminants especially aromatic hydrocarbons in aqueous media under light irradiations (Szczepanik 2017). When UV/Vis light is used to irradiate TiO_2 nanoparticles and composites, it causes electron-hole charge-pair separation by the transfer of electrons from the valence band (VB) of TiO_2 to its conduction band (CB) (Nassar 2019). The photocatalytic efficiency of TiO_2 is based on the formation of the electron-hole pairs and rate of their recombination (Li et al. 2015). By shortening the distance between the valance and conduction bands and delaying their rate of recombination, the efficiency of catalytic nanoparticles can be improved (Simon et al. 2016; Tian et al. 2018). This can be done either, by doping the TiO_2 with transition metals such as Pt, Cu, Ag, Bi, and Au into or by making its composites materials with different semiconductors (Qi et al. 2017).

Currently, the introduction of Graphene Oxide (GO) is the best and the most efficient way to enhance the efficiency of TiO_2 toward the contaminant degradation in aquatic media due to the high surface area of GO (Viet et al. 2021). However, the molecular structure of GO contains huge number of oxygens based groups i.e., epoxide and hydroxyl that are responsible for great decrease of electronic properties. In order to produce the highly effective GO based TiO_2 photocatalytic nanoparticles, the reduction of GO is required. It is reported in the literature that hydrazine and sodium borohydride are good reductants being used for reducing GO to rGO. However, due to their toxic effects on both humans and environment, it is very necessary to propose an eco-friendly technique for titania-reduced graphene oxide nanocomposites synthesis (Preetha et al. 2022). Different techniques are utilized

for the preparation of titania-reduced graphene oxide that includes; simple mixing and sonication technique, sol-gel method, photochemical method, radiolytic reduction method, and hydrothermal method (Gupta and Melvin 2017). Hydrothermal route is considered the most efficient and easy way for titania-reduced graphene oxide synthesis due to the good morphological properties of as-synthesized nanocomposite material by this technique. (Balsamo et al. 2021) used one-pot method for the synthesis of TiO_2 -rGO photocatalysts. Different characterization techniques like, Raman, FTIR, UV-DRS, and nitrogen adsorption-desorption were employed for determining mechanical, optical, and textural characteristics of TiO_2 -rGO. The synthesized material was used for 2,4-Dichlorophenoxyacetic acid (2,4-D) degradation in aquatic media under light irradiations. Their findings revealed 97% removal of 2,4-D by as-synthesized TiO_2 -rGO in 3 h showing the low efficiency of TiO_2 -rGO toward 2,4-D degradation. Nada et al. (Nada et al. 2018) synthesized titania-magnetic reduced graphene oxide nanocomposites (MRGT) and utilized these materials for the photocatalytic degradation of tartrazine (TZ) in aquatic media. Their findings showed that under visible light irradiations for 3 h, catalyst amount of 0.2 g/L, 60 mL of 50 ppm dye, 95% of the selected dye, TZ was successfully degraded that showed the high photocatalytic efficiency of MRGT compared to magnetic reduced graphene oxide and titania nanoparticles that showed 35 and 10% degradation of TZ respectively.

In this study, we paid attention to synthesize the highly efficient, light responsive Titania/reduced Graphene Oxide nanocomposites (TiO_2/rGO) by simple hydrothermal technique. For analysis of as-synthesized TiO_2/rGO , different characterization techniques (XRD, SEM, EDX, TEM, HRTEM, TGA, UV-DRS, PL, EIS, BET) were employed that confirmed the crystalline nature, good morphology, high thermal stability, low band gap energy, high surface area, and high concentration of $\bullet\text{OH}$ formation by TiO_2/rGO . The photocatalytic efficiency of these materials were determined toward brilliant green (BG) removal in different water systems (deionized water, tap water, synthetic wastewater, and industrial samples). The effects of different parameters/factors like catalyst amount, initial solution pH, and the role of oxidant like peroxymonosulfate (PMS) in the contaminant degradation was also studied. Some scavenger experiments were also performed in order check the role of various reactive species ($\bullet\text{OH}$, $\text{SO}_4\bullet^-$, h^+ , and $\text{O}_2\bullet^-$) in BG degradation. Reduced graphene oxide (rGO) was selected for making its composite with TiO_2 because of the large surface area, very low water solubility, and high electronic properties (M. Chen et al. 2013).

Materials and methods

Chemicals

Titanium tetrakisopropoxide ($C_{12}H_{28}O_4Ti$, 98%), sodium nitrate ($NaNO_3$, 99.0%), perchloric acid ($HClO_4$, 60%), and terephthalic acid ($C_8H_6O_4$, 97%) were obtained from Daejung Korea. Ethanol (C_2H_5OH , 99.8%), hydrogen peroxide (H_2O_2 , 35%), and Oxone salt ($KHSO_5 \cdot 0.5KHSO_4 \cdot 0.5K_2SO_4$) were provided by Sigma-Aldrich. Glacial acetic acid (CH_3COOH , 99.8%), sulfuric acid (H_2SO_4 , 98.0%), sodium hydrogen carbonate ($NaHCO_3$, 99%), potassium permanganate ($KMnO_4$, 99.0%), sodium hydroxide ($NaOH$, extra pure), ter-Butanol ($C_4H_{10}O$, 99.0%), and graphite powder (99.0%) were purchased from Scharlau Spain. Sodium chloride ($NaCl$, 99.5%) and potassium iodide (KI , 99.8%) were supplied by Merck. Isopropanol (C_3H_8O , 99.9%) and sodium carbonate (Na_2CO_3 , 99.8%) were supplied by Acros Belgium. Brilliant green ($C_{27}H_{34}N_2O_4S$, 93%) was provided by Aldrich Chemical Company.

Synthesis of TiO_2 nanoparticles

TiO_2 nanoparticles were obtained by hydrothermal method. For synthesis of TiO_2 nanoparticles, 20 mL of titanium tetrakisopropoxide was taken in an ice bath at $0^\circ C$. About 36 mL of glacial acetic acid was slowly added into it. The said mixture was stirred for 20 min. After 20 min of continuous stirring, 170 mL of distilled water was added into it. After the addition of distilled water, the mixture was vigorously stirred for 1 h followed by ultrasonication for 30 min. After the completion of sonication process, the mixture was once again vigorously stirred for 4 h. Afterwards, the mixture was transferred to the Teflon jar that was put inside the stainless steel autoclave. The autoclaves were put inside in an oven and the samples were heated at $150^\circ C$ for 12 h. After 12 h of heating in an oven the autoclaves were taken out from oven. The contents of the Teflon jars were splashed numerous times with distilled water. After washing, the precipitate was vacuum dried at $95^\circ C$ for 3–4 h (Collazzo et al. 2011). The dried samples were taken out from oven and grinded with the help of mortar and pestle. The grinded samples were calcined in a furnace at four dissimilar temperatures of $450^\circ C$, $550^\circ C$, $650^\circ C$, and $750^\circ C$ at the ramping of $10^\circ/min$ for 3 h.

Synthesis of GO

Modified Hummer's method was used for the synthesis of Graphene oxide (GO) using graphite powder as precursor. For this purpose, 46 mL of H_2SO_4 was taken in

500 mL volumetric flask. The volumetric flask was placed over magnetic stirrer inside the ice bath and about 4 g of $NaNO_3$ was added slowly into it with continuous stirring. After the addition of $NaNO_3$, 1 g of graphite powder was poured slowly into the mixture and the stirring was done for 60 min. After 60 min of continuous stirring 6 g of $KMnO_4$ was added into it and the reaction mixture was stirred for 30 min. The ice bath was detached after 30 min and the mixture was kept on stirring at a temperature of $35^\circ C$ till the brown colored paste was formed. The brownish paste was left overnight. After that, 100 mL of distilled water was added into the mixture followed by continuous stirring for about 1 h at a temperature of $98^\circ C$. About 15 mL of H_2O_2 was poured to the mixture after 1 h of continuous stirring that results in the formation of suspension. The suspension was once again stirred for 10 min and was diluted with distilled water so that the precipitate may get settled down. The mixture was washed several times till the formation of black precipitate occurred at pH 7. The black precipitates were transferred to large Petri dish and kept in vacuum oven at a temperature of $80^\circ C$ for dryness. After vacuum dryness the black sheet of GO was obtained (Ambrosi et al. 2012).

Synthesis of titania/reduced graphene oxide nanocomposites (TiO_2/rGO)

Simple hydrothermal technique was utilized for various percent TiO_2/rGO (0.5%, 1%, 2%, 3%) synthesis by changing the concentration of GO while the concentration of TiO_2 was kept constant during the experiments. These samples were named as TrG0.5, TrG1, TrG2, and TrG3 for 0.5%, 1%, 2%, and 3% TiO_2/rGO nanocomposites respectively. In order to prepare TrG0.5, 2.5 mg of GO was taken in a beaker and dissolved it in a 50 mL of distilled water using ultra sonicator for 20 minutes. The same process was applied for the formation of TrG1, TrG2, and TrG3 composites formation by taken 5 mg, 10 mg, and 15 mg of GO respectively. After the formation of GO solution, 500 mg of TiO_2 (calcined at $650^\circ C$) was poured slowly into the mixture. Magnetic stirring was done for 2 h. After 2 h of continuous stirring, the mixture (H_2O , GO, TiO_2) was transferred to Teflon autoclave and placed inside the oven at a temperature of $150^\circ C$ for a reaction time of 5 h. After 5 h, the oven was turned off and the autoclave containing as-synthesized material was taken out from it. The obtained sample was recovered by centrifugation, splashed numerous times with distilled water, followed by vacuum dryness in an oven at a $60^\circ C$ for 12 h. Different weight percent TiO_2/rGO were successfully obtained after 12 h of vacuum dryness (P. Wang et al. 2013). The overall mechanism of nanocomposite formation is depicted in Fig. 1



Fig. 1 Experimental procedure for step-wise synthesis of TiO₂/rGO

Characterization of as-synthesized TiO₂ and TiO₂/rGO

The morphology of TiO₂ and TiO₂/rGO was determined by scanning electron microscopy (SEM) (JEOL, JSM-5910) and transmission electron microscopy (TEM) (JEM-2100). The elemental analysis and percent purity of as-synthesized materials were determined by Energy-dispersive X-ray (EDX) technique (EX-2300BU, JEOL). The X-ray diffraction technique (XRD, PANalytical) was carried out for determining the crystallinity, phase composition, and crystallite size using Rigaku D/max-RB instrument having Cu-K α radiation ($\lambda = 1.54\text{\AA}$), scan rate of $0.03^{\circ}2\theta\text{ s}^{-1}$ operated at 45 kV and 100 mA. To check the thermal stability of as-synthesized nanoparticles, thermal gravimetric analysis (TGA) was carried out on TG-DTA, Perkin-Elmer system. For band gap energy (E_g) determination, the ultra-violet diffuse reflectance spectroscopy (UV-DRS) was carried out on Perkin Elmer Lambda 35 UV-Vis spectrometer (PerkinElmer

UV/VIS/NIR Spectrometer Lambda 1050) using BaSO₄ as a reference material. The point of zero charge (PZC) was determined by salt addition method. The production of hydroxyl radicals ($\bullet\text{OH}$) were confirmed by PL analysis of irradiated photocatalysts in aqueous solution using fluorescence spectrometer (PerkinElmer LS 45). Electrochemical impedance spectroscopy (EIS) was used for determining resistance and lifetime of charge carriers and charge transport using Corrtest Potentiate/Galvanostat (CS310). The surface area of as-synthesized TiO₂ and TrG2 was determined by BET analysis (Quantachrome® ASiQwin™- Automated Gas Sorption Data, Acquisition and Reduction, 1994–2017, version 5.21)

PL analysis

This technique was utilized for the confirmation of $\bullet\text{OH}$ formation during the photocatalytic process. For this purpose, 50 mL of 3.5×10^{-4} M terephthalic acid (TA), 50 mL of 2

$\times 10^{-3}$ M sodium hydroxide (NaOH) and 10 mg of TiO_2/rGO nanocomposite was taken in petri dish. The same procedure was performed for TiO_2 nanoparticles also except that TiO_2 was taken instead of TiO_2/rGO composite material. The mixture in the Petri dish was placed under UV lamp (UV-254 nm) for 100 min. Irradiation of TiO_2 and TiO_2/rGO produced $\bullet\text{OH}$ (Eq. (1) and (3)) that on reaction with TA produced 2-hydroxyterephthalic acid (TAOH) (Eq. (2) and (4)). The fluorescence intensity has direct relation with the concentration of TAOH produced during the process. Hence, it confirmed that the $\bullet\text{OH}$ have been successfully produced.



Point of zero charge (PZC) determination for as-synthesized TrG2

Before performing the experiments in various media (acidic and basic), the PZC of the as-synthesized TrG2 was determined by salt addition method. Figure 2 shows the PZC of as-synthesized TrG2 by salt addition method. In a typical experiment 40 mL of NaNO_3 (0.1 M) was taken in ten different reagent bottles. pH of the solutions were adjusted from 3 to 12 by means of 0.1 M HNO_3 and NaOH respectively.

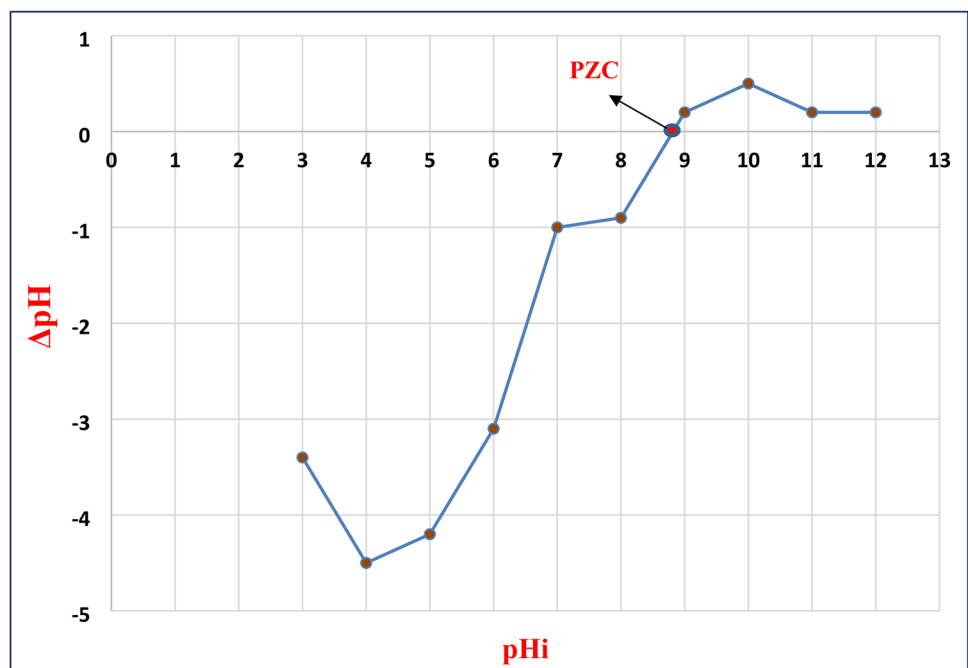
After pH adjustment, 20 mg of as-synthesized TrG2 was added in each reagent bottle. The reagent bottles were then placed inside a shaker at a speed of 150 rpm for 24 h. After 24 h of shaking, filtrations of all the ten mixtures were performed. Once again, the pH of the filtrate was determined accordingly. Then, by using Equation (5), ΔpH values were determined. Finally, ΔpH values were plotted against pHi values and the PZC of the material was determined accordingly. In our case, the PZC of TrG2 was found to be 8.8 (Bakatula et al. 2018).

$$\Delta\text{pH} = \text{pHi} - \text{pHf} \quad (5)$$

Photocatalytic activity of as-synthesized TiO_2 , TiO_2/rGO , and $\text{TiO}_2/\text{rGO}/\text{PMS}$ in terms of brilliant green degradation under UV irradiations

The efficiency as-synthesized materials were determined toward the degradation of brilliant green (BG) in aqueous media both in the presence as well as in the absence of PMS under UV irradiations. The photocatalytic reactor comprised of closed opaque box having magnetic stirrer (BANTE, MS300) in order to carry out the uniform mixing of the mixture and to ensure unvarying glow of UV irradiations over the mixture (Dong et al. 2022). For experimental work, 100 mL ($10 \text{ mg} \cdot \text{L}^{-1}$) of BG was taken in a 120-mL Petri dish containing the as-synthesized material. Prior to photocatalytic degradation of BG, the continuous stirring of the mixture was carried out in dark for 30 min to attain

Fig. 2 PZC determination of as-synthesized TrG2 using salt addition method.



the adsorption and desorption equilibrium of BG over the material surface. After 30 min of continuous stirring in dark, the UV irradiation was allowed to strike the reaction mixture to perform the photocatalytic degradation of BG dye. The different initial concentrations of TrG2 (5 mg/100 mL, 10 mg/100 mL, 15mg/mL, 20 mg/mL) and PMS (0.1 mM, 0.5 mM, 1 mM, 1.5 mM, 2 mM) were used during the experiments to find the optimum conditions. The degradation experiments were also performed in various media (neutral, acidic, basic) to find the effect of pH on the degradation of BG. For pH adjustment HClO₄ and NaOH were used. The radical quenching experiments were carried out using isopropanol (•OH scavenger), benzoquinone (O₂•⁻ and O₂ scavenger), EDTA (h⁺ scavenger), and ethanol (•OH and SO₄•⁻ scavenger) for determining the role of various radical species involved in the degradation of the selected contaminant. Furthermore, in order to check the efficiency of TiO₂ and TiO₂/rGO, the degradation experiments were performed in different types of water like deionized water (DI), ordinary tap water (TPW), synthetic/lab made wastewater (SWW), and industrial wastewater (IWW) samples.

Quantitative analysis of BG

The quantitative determination of BG after photocatalytic degradation was studied using SpectroVis Plus. For this purpose, first calibration plots were drawn. After calibration plot, degradation of BG under UV light using TiO₂ and TiO₂/rGO was recorded with the help of SpectroVis Plus. At specific time interval (20 min each), 3 mL of sample was taken from Petri dish, filtered with the help nylon syringe filter (0.45 μm). After filtration the sample was quantitatively analyzed using SpectroVis Plus. The absorbance spectra were obtained and from that spectrum, the concentration at time “t” (C_t) was calculated using straight line equation (y = mx). The percent degradation of the BG after each time interval was obtained using the degradation formula (Eq. 6).

$$\% \text{ Degradation} = \frac{C_0 - C_t}{C_0} \times 100 \quad (6)$$

In Equation (6) “C₀” is the starting concentration of the contaminant (BG) and “C_t” is its final concentration at time “t” (Le and Tran 2020).

By-product analysis by chromatographic technique

Qualitative analysis of the BG by-products was performed by Gas chromatography combined with mass spectrometry using GC-MS, QP.2010 plus, Shimadzu, Japan with DB-5MS column (30 m 0.25 mm 0.25 m). The operating conditions were as followed: pressure = 68.9 kPa, total flow = 40 mL/min, column flow = 1.27 mL/min, linear velocity =

40.7 cm/sec, purge flow = 7 mL/min, sample volume = 1 μL. The injection mode was splitless, the flow control mode was linear velocity, the mobile phase was He gas, and the injection temperature was 240°C. The oven temperature was set to start at 40°C, increase to 80°C at a ramping rate of 10°C min⁻¹, then increased to 280°C at a ramping rate of 4°C min⁻¹, and hold for 1 min. The range of *m/z* values were from 40 to 800.

Results and discussion

Characterization of as-synthesized GO, rGO, TiO₂, and TrG2

The morphological characterization of as-synthesized TiO₂, rGO, and TrG2 were carried out using SEM analysis. The SEM images of TiO₂ nanoparticles in Fig. 3(A) confirmed its crystalline morphology with irregular shape crystals in which some crystals are large while some are small in size. Somewhere the agglomeration of particles can be seen in SEM images. The particle size of TiO₂ was ranged from 2 to 40 μm. The mean particle sizes calculated from these images were found to be 6.4 μm (Fig. 3(A) inset). In the case of rGO, the large flower like sheets are observed (Fig. 3(B)). These rGO sheets are randomly arranged somewhere agglomeration can also be seen. The porosity in rGO sheets can also be found in these structures. The particle size of rGO was ranged from 5 to 10 μm. The mean particle size of rGO was found to be 7.8 μm (Fig. 3(B) inset). In comparison to TiO₂ and rGO, the SEM images of the TrG2 material show sheet-like structures in which TiO₂ particles are attached (Fig. 3(C)). The irregularity of particles and porosity can also be seen in these images. Furthermore, the random distribution of TiO₂ nanoparticles over rGO sheets can also be observed. The particle size of TrG2 was ranged from 10 to 100 μm having the mean particle size of 34.4 μm (Fig. 3(C) inset).

The TEM analysis was performed to get more detailed information of the as-synthesized TrG2 nanocomposite material. Figure 4(A) and (B) shows the large rGO sheets over the surface of which TiO₂ nanoparticles are attached. Figure 4(A) and (C) confirms the unequal distribution of TiO₂ nanoparticles over rGO sheets. TiO₂ nanoparticles show variation in size. The agglomeration of TiO₂ nanoparticles over rGO sheets can also be seen in these images (Fig. 4(A) and (D)). Furthermore, these images revealed the porous nature of as-synthesized TrG2 nanocomposite (Fig. 4(C)).

The XRD analysis of as-synthesized GO, rGO, TiO₂, and TrG2 are depicted in Fig. 5(A). The broad peak appeared at 2θ = 12.6° in the case of GO confirmed that GO has been successfully synthesized with amorphous morphology

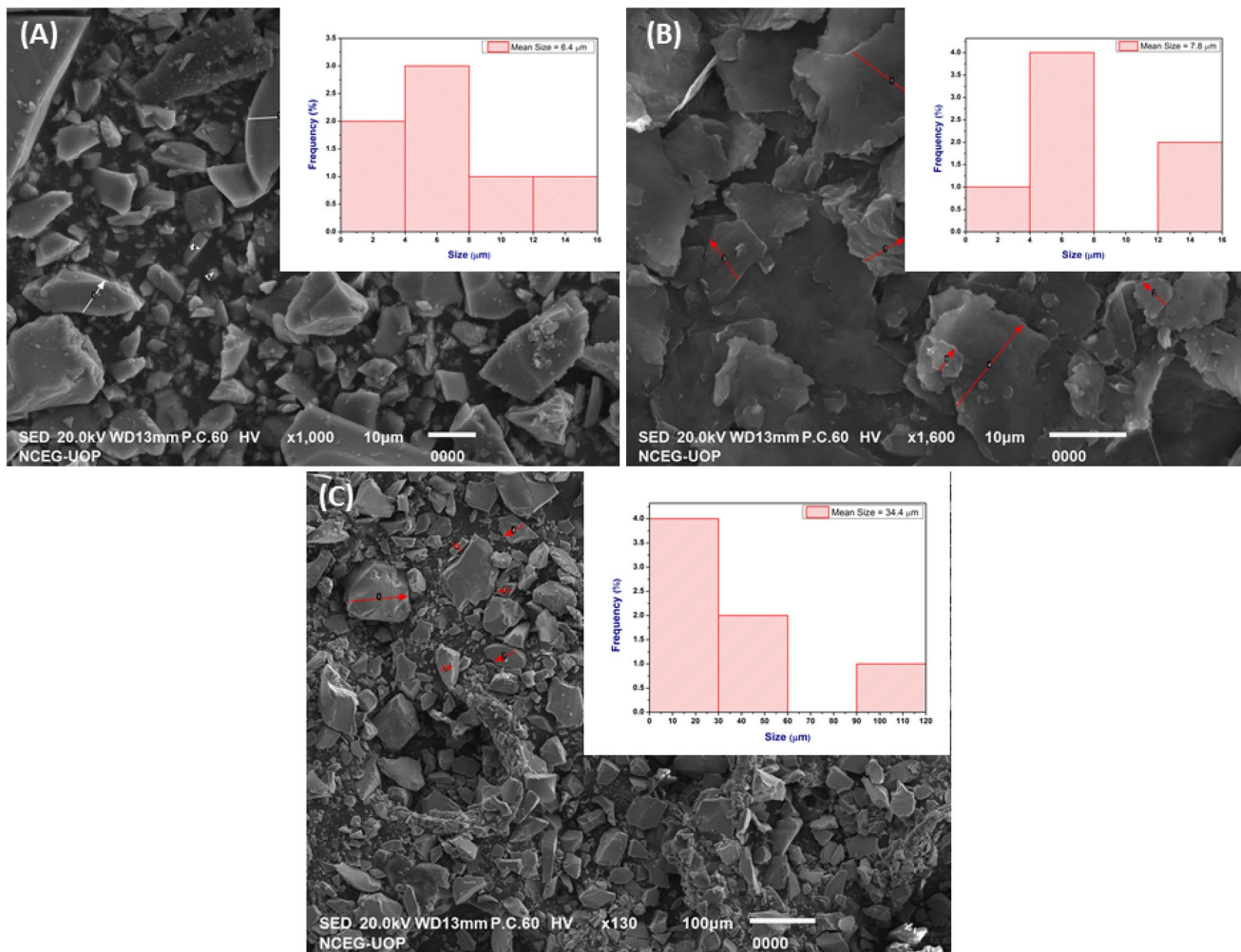


Fig. 3 SEM analysis of as-synthesized **A** TiO₂, **B** rGO, **C** TrG2 (inset; particle distribution graphs).

(Hanifah et al. 2019). The JCPDS 00-032-1665 confirmed that the GO sheet belongs to monoclinic system ($\alpha = \gamma = 90^\circ \neq \beta$). The small peak still observed at $2\theta = 26^\circ$ indicates that graphene oxide is not fully interconnected with oxygen atoms. In the case of rGO, a broad peak appeared at $2\theta = 20\text{--}30^\circ$. The shifting of peak from 12.6 to 25.6° showed that the GO has successfully reduced to rGO (Sun et al. 2018). The XRD spectra of TiO₂ nanoparticles in Fig. 5 showed the successful formation of TiO₂ nanoparticles with high crystallinity and tetragonal geometry (JCPDS 01-084-1285 and 00-034-0180). The peaks at $25^\circ, 27^\circ, 38^\circ, 48^\circ, 54^\circ, 55^\circ, 62^\circ, 69^\circ,$ and 75° confirmed the anatase ($25^\circ, 38^\circ, 48^\circ, 54^\circ, 62^\circ, 69^\circ, 75^\circ$) and rutile ($27^\circ, 55^\circ, 75^\circ$) phases of titania. The XRD pattern of as-synthesized TrG2 showed the successful formation of nanocomposite material with crystalline morphology (JCPDS 01-073-1764 and 00-034-0180). The crystals belong to tetragonal system ($\alpha = \beta = \gamma = 90^\circ$). No extra peak for rGO in XRD spectra means that the guest material (rGO) has gone into the interior of the

TiO₂ crystals and has made strong covalent bond with the host material (TiO₂) or it may be due to the small amount of rGO in the composite material (Sher Shah et al. 2012). The crystallite size (D) was obtained from these XRD spectra using the well-known Scherrer's equation (Eq. 7).

$$D = K\lambda/\beta\cos\theta \quad (7)$$

In Eq. 7 “ K ” is the coefficient (0.89), “ D ” is the average crystallite size in nm, “ θ ” is the maximum diffraction angle, “ β ” is the full width at half maximum (FWHM) of the diffraction peak, and “ λ ” is the X-ray wavelength in nm. In our study, the crystallite size of GO, rGO, TiO₂, and TrG2 was found to be 1.86, 1.10, 31.5, and 18.4 nm respectively. Furthermore, high-resolution transmission electron microscopy (HRTEM) image of TrG2 (Fig. 5(B)) clearly displays the lattice spacing of 0.35 nm that belongs to (101) crystal plane of the anatase TiO₂ and thus in good agreement with the XRD

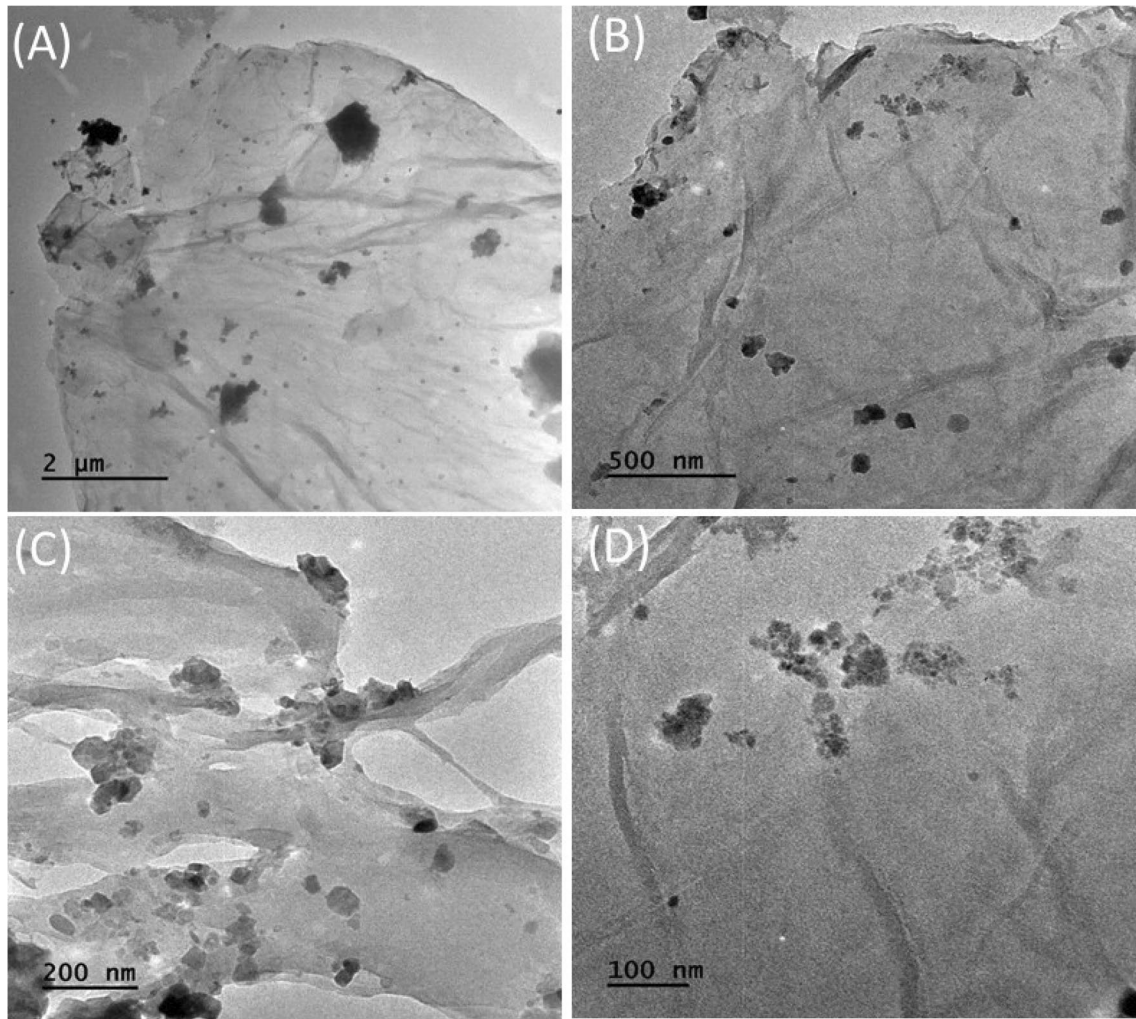
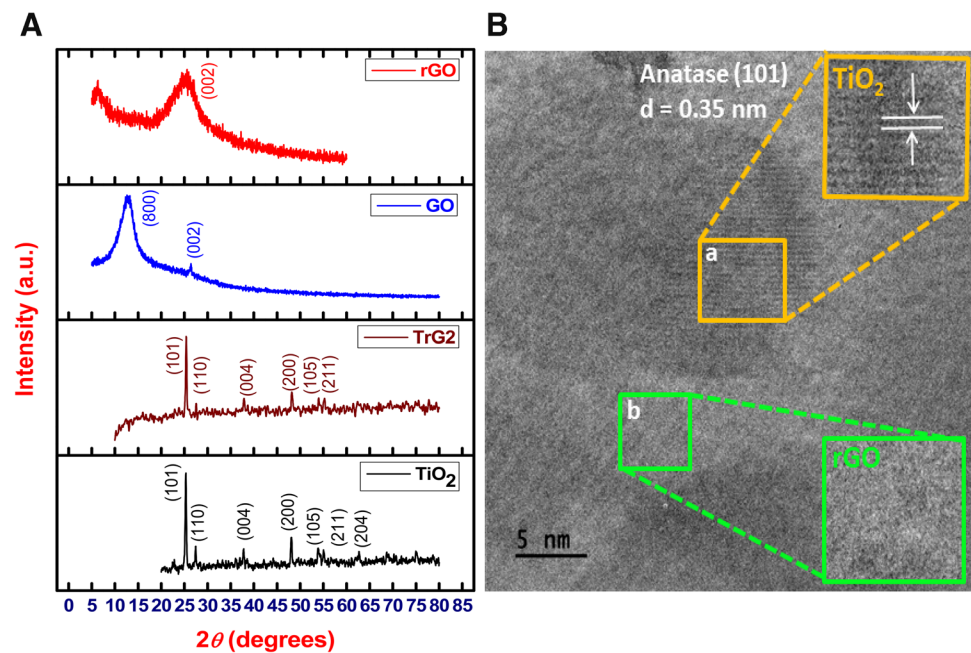


Fig. 4 TEM analysis of as-synthesized TrG2.

Fig. 5 **A** XRD analysis of as-synthesized GO, rGO, TiO₂, and TrG2. **B** HRTEM analysis of as-synthesized TrG2 material.



results (Nainani and Thakur 2016). The presence of such anatase TiO_2 with dominant (101) facets in TrG2 sample exhibits high photoactivity because the composite photocatalyst has $\text{O}_2^{\bullet-}$ on its surface (Gul et al. 2020). Moreover, the lattice spacing are not very much clear which is due to the wrapping of rGO on the surface of TiO_2 nanoparticles (Tolosana-Moranchel et al. 2019a).

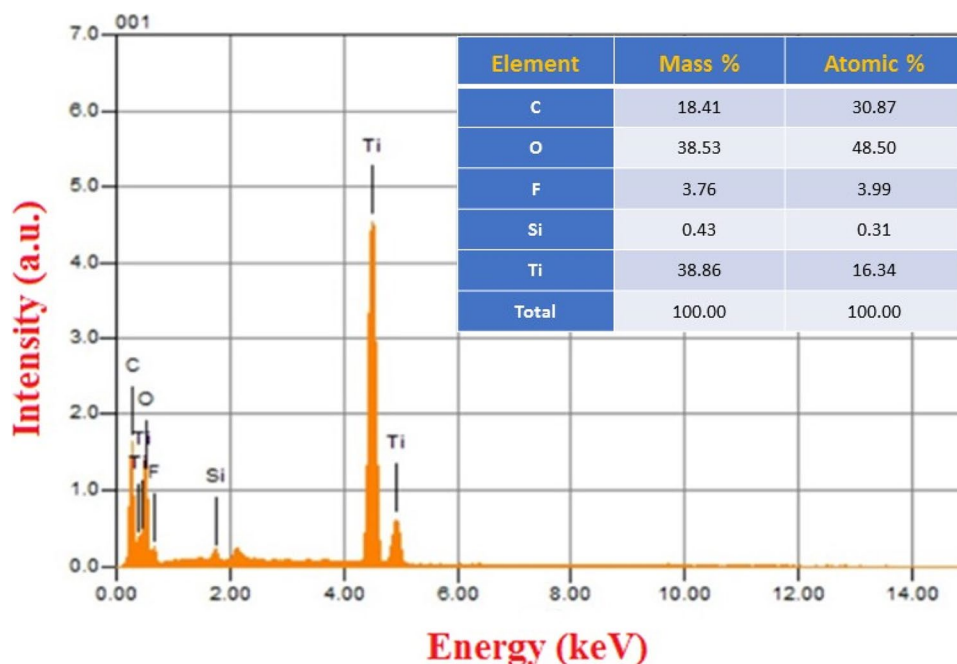
The EDX technique was carried out for elemental analysis of as-synthesized TrG2 material. Details of the EDX spectrum of the as-synthesized TrG2 values measured in weight and atomic % are listed in Fig. 6 inset which shows the percentage of titanium (Ti) (38.86%) followed by oxygen (38.53) and carbon (18.41%). The presence of high percentage of titanium and oxygen confirmed the formation of titanium dioxide while the high carbon content is attributed to the reduced graphene oxide sheets in TrG2 nanocomposite material (Irshad et al. 2020). The small amount of other elements like fluorine (3.76%), and silicon (0.43%) can also be seen in the EDX spectrum that might be came from the glassware used during material synthesis or impurities present in chemicals that were utilized during sample preparation.

The thermal stability of as-synthesized rGO, TiO_2 , and TrG2 was determined by thermogravimetric analysis (TGA) under argon gas at a ramping temperature of $30^\circ\text{C}/\text{min}$ from 25 to 900°C . Figure 7 shows the TGA analysis of as-synthesized rGO, TiO_2 , and TrG2 respectively. In the case of rGO, the initial decrease in weight ($\sim 8\%$) at $30\text{--}180^\circ\text{C}$ temperature attributes to the removal of physically adsorbed water molecules. The second loss in weight ($\sim 13.6\%$) in the temperature range of $180\text{--}400^\circ\text{C}$ is attributed to the

loss of oxygenated groups (hydroxyl, carboxyl, and epoxides) attached with rGO sheets. The third weight loss after 400°C is due to the destruction of the carbon skeleton of rGO sheets (Hu et al. 2012). The initial weight loss in the case of TiO_2 (Fig. 7) attributes to the loss of alcohol (isopropanol) molecules followed by the dehydration of water molecules (Kim et al. 2008). The third weight loss attributes to the loss of acetic acid that was utilized during material synthesis (Pichon et al. 2006). These results revealed that about 30.7% of the weight loss occurred during heating the sample from 25 to 900°C showing the high thermal stability of as-synthesized TiO_2 nanoparticles. In the case of TrG2 (Fig. 7), the initial weight loss attribute to the evaporation of alcohols and water followed by the loss of acetic acid. The third weight loss attributes to the loss of rGO that occurred in the temperature range of $500\text{--}650^\circ\text{C}$ (Gavgani et al. 2014). These results revealed that during the hydrothermal process the stability of graphene oxide being thermally unstable increased and about 29.8% of the weight loss occurred during heating the sample from 25 to 900°C . The high thermal stability of rGO in the TrG2 is due to the strong contact of rGO with TiO_2 nanoparticles.

Figure 8 shows the UV-DRS spectra of as-synthesized TiO_2 and TrG2 by plotting photon energy ($h\nu$) vs $(\alpha h\nu)^2$ (eV cm^{-1})². The spectra for TiO_2 and TrG2 were extrapolated at x-axis and the point at which these spectra touches on x-axis shows the band gap energy (E_g) of TiO_2 and TrG2, respectively. It can be seen from Fig. 8 that upon the incorporation of rGO in the TiO_2 system the E_g of TiO_2 decreases from 3.38 to 3.12 eV. The decrease in band gap energy in the case of TrG2 is because of the incorporation of new energy band

Fig. 6 EDX spectrum of as-synthesized TRG2 (inset; Showing the percent composition of each element in as-synthesized TrG2).



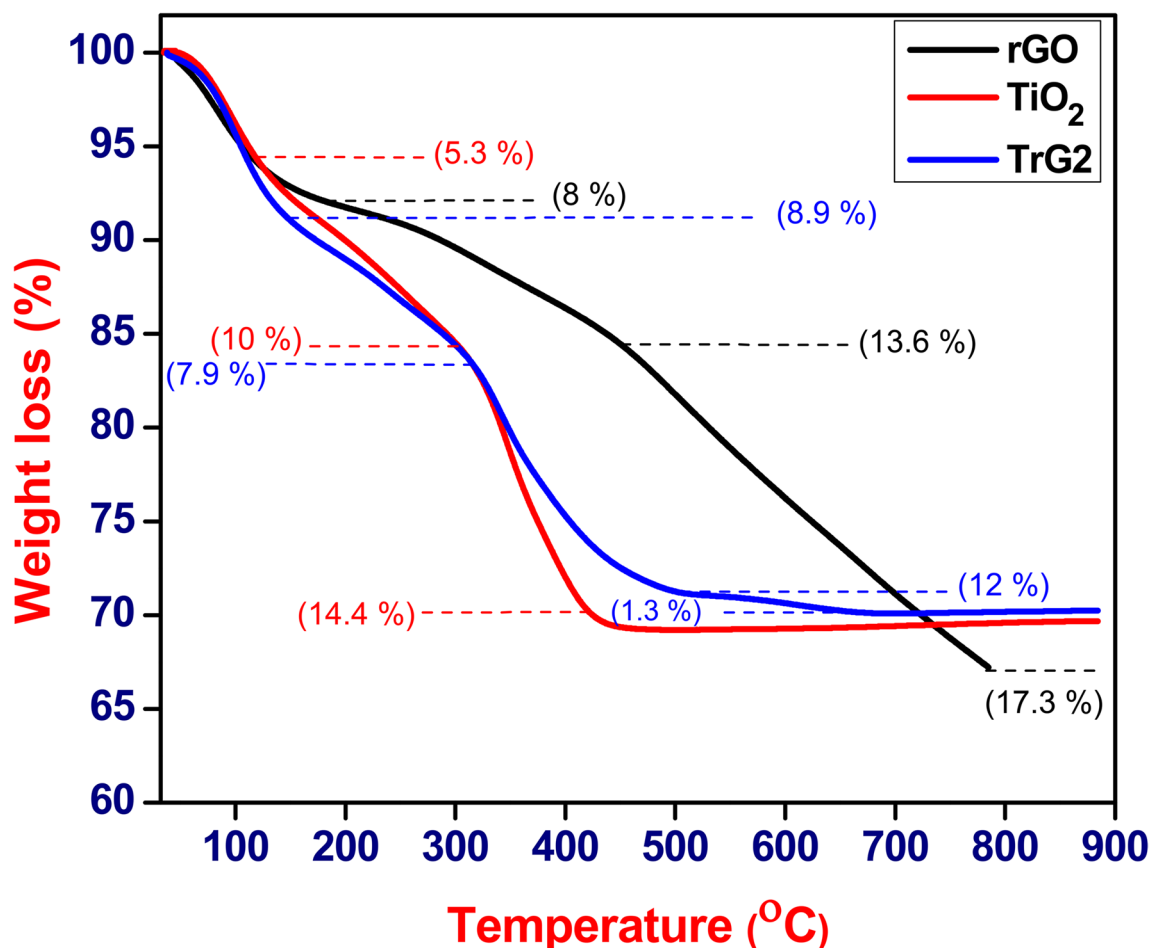


Fig. 7 TGA analysis of as-synthesized rGO, TiO₂, and TrG2.

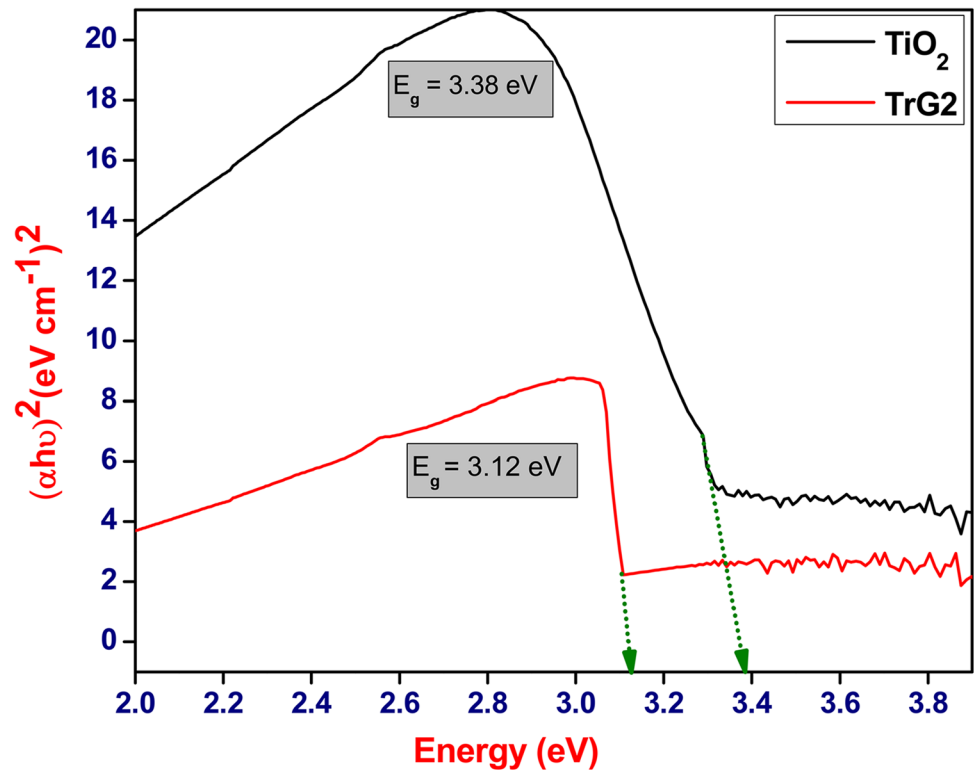
of rGO closed to the conduction band of TiO₂ (Tolosana-Moranchel et al. 2019b).

Hydroxyl radical ($\bullet\text{OH}$) formation during the photocatalytic process was confirmed by the PL analysis of as-synthesized TiO₂ and TrG2. The PL analysis was carried out in the wavelength range of 350 to 580 nm. Figure 9 shows the PL analysis of as-synthesized TiO₂ and TrG2 respectively. The appearance of broad peak in the case of TiO₂ and TrG2 confirmed that $\bullet\text{OH}$ have been successfully produced during the photocatalytic process. The high peak intensity in the case of TrG2 is due to the high concentration of $\bullet\text{OH}$ formation. The high concentration of $\bullet\text{OH}$ production in the case of TrG2 indicates the decrease in electron-hole pair recombination because of the incorporation of reduced graphene oxide sheet near the conduction band of TiO₂. The rGO sheet act as electron sink or electron reservoir for the photogenerated electrons of the TiO₂ produced by the transfer of electrons from the valence band (VB) of TiO₂ to the conduction band (CB) of TiO₂ under UV irradiations (Pei et al. 2014).

The specific surface area, pore size, and volume distributions of the as-synthesized TiO₂ and TrG2 materials were

studied by BET analysis. Figure 10 shows the corresponding N₂ adsorption-desorption isotherms for as-synthesized TiO₂ and TrG2 materials. The results revealed that both TiO₂ and TrG2 materials follow the type-IV isotherm with the hysteresis loops at $0 < P/P_0 < 1$, proving the mesoporous nature of the as-synthesized materials (Khavar et al. 2018). For each sample, the inset figure in adsorption-desorption isotherms indicates the corresponding BJH pore size distribution curves that also confirm the mesoporous nature of TiO₂ and TrG2 materials because the pores presents in these samples are in the mesoporous range (2–50 nm) and exhibit wide pore size distribution. Table 1 represents the BET surface area (S_{BET}), pore volume (V_p), and pore diameter (D_p) for as-synthesized TiO₂ and TrG2 materials. It can be seen from the Table 1 that compared to TiO₂ materials, the as-synthesized TrG2 possess high S_{BET} (65.698 m²/g), V_p (0.182 cm³/g), and D_p (13 nm). The increase in surface area of TrG2 compared to TiO₂ is due to the successful incorporation of rGO in the TrG2 material that significantly improved the surface area (Khavar et al. 2018; Kovačić et al. 2020; P. Wang et al. 2013).

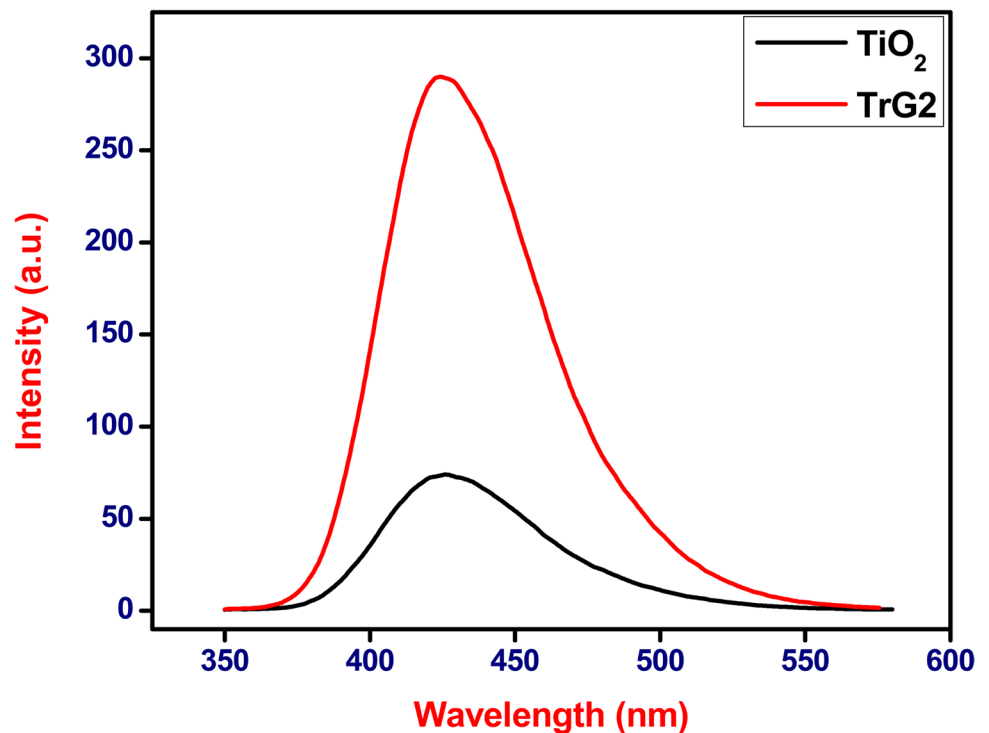
Fig. 8 UV-DRS analysis of as-synthesized TiO₂ and TrG2.



Furthermore, the electrochemical impedance spectroscopy (EIS) measurement was utilized to explore the charge-transfer/recombination behavior of TiO₂ and TrG2 samples (Fig. 11). The small semicircle diameter shown by TrG2

compared with the bare TiO₂ in the EIS Nyquist plot, indicating the lower resistance of charge transfer (Ouedraogo et al. 2022). The better electrical conductivity of TiO₂/rGO interface in TrG2 promotes the spatial charge separation and

Fig. 9 PL analysis of as-synthesized TiO₂ and TrG2.



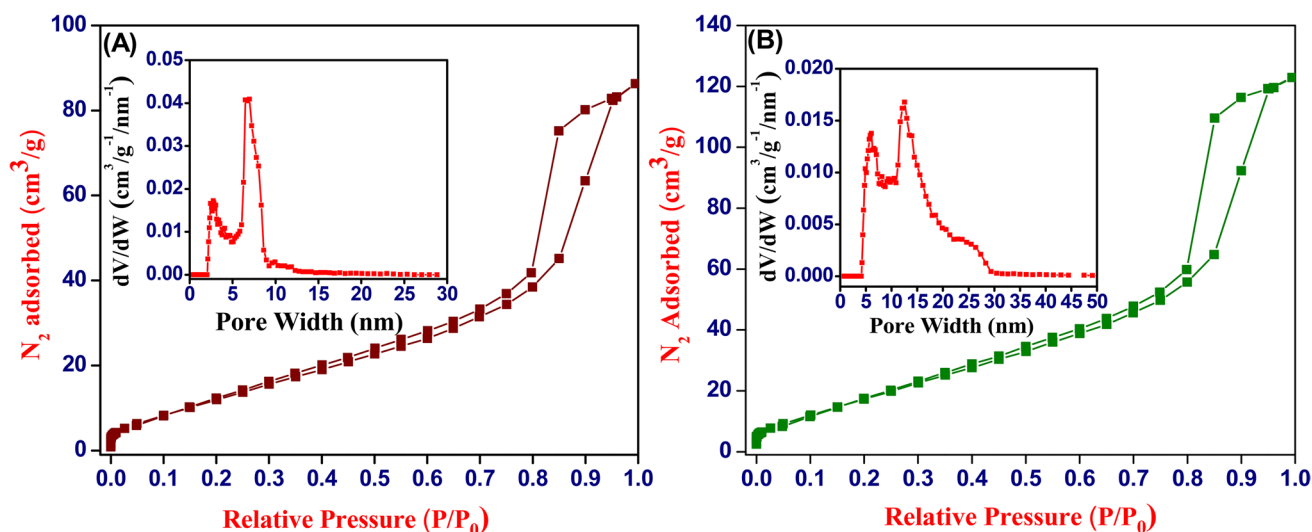


Fig. 10 BET analysis of as-synthesized TiO₂ (inset pore size distribution curve) (A). TrG2 nanocomposite (inset pore size distribution curve) (B).

transfer. Moreover, the high $\bullet\text{OH}$ concentration production for TrG2 sample in PL analysis (Fig. 9) also supports the decrease in electron-hole pair recombination rate because of the incorporation of reduced graphene oxide sheet near the conduction band of TiO₂. Therefore, it could be anticipated that TrG2 photocatalyst would show better photodegradation property compared with the bare TiO₂, due to the fast photo-induced charge carrier's separation, high electrical conductivity, and low resistivity that initiates from the combined effect of rGO and TiO₂ in TrG2 sample (Mansingh et al. 2022; Rahman et al. 2018).

Mechanism of photocatalytic performance of as-synthesized materials

The photocatalytic efficiencies of TiO₂ and TiO₂/rGO samples were investigated toward brilliant green (BG) degradation under UV irradiations in aqueous media. Prior to this, photolysis of BG was carried out in order to determine the stability of BG under UV irradiations. Figure S1 (supporting information) shows the degradations of BG in the presence of UV irradiations. The results showed that under UV light illumination for 100 min, only 7.7% degradation of BG (10

mg.L⁻¹) was achieved that confirmed the high stability of BG dye under UV irradiations (Sood et al. 2015).

After photolysis, the photocatalytic efficiencies of as-synthesized TiO₂ and different weight percent TiO₂/rGO (0.5%, 1%, 2%, and 3%) were evaluated toward BG degradation in aqueous media at a reaction time of 100 min. Figure 12 shows the efficiency of as-synthesized photocatalytic materials (TiO₂ and TiO₂/rGO). The results revealed only 53% degradation of BG under UV irradiations, at a reaction time of 100 min by as-synthesized TiO₂ with the k_{app} of 0.006 min⁻¹. In the case TiO₂/rGO, the degradation of BG increases significantly. It was observed that under UV irradiations for 100 min, 84.4, 90, and 91.4%, degradation of BG takes place with the k_{app} of 0.0164, 0.0203, and 0.023 min⁻¹ for as-synthesized TrG0.5, TrG1, and TrG2 respectively. The photocatalytic efficiency of composite material increases as the rGO content in the composite material increases. The highest efficiency was observed for TrG2 with the k_{app} of 0.023 min⁻¹ that could be attributed to its small crystallite size (18.4 nm), high crystallinity, low band gap energy ($E_g = 3.12$ eV) and the decrease in electron hole pair (e^- , h^+) recombination, compared to as-synthesized TiO₂ nanoparticles. However, only 34.5% degradation of BG was observed for TrG3 under UV irradiations for 100 min with the k_{app} of 0.0044 min⁻¹ (Fig. 12; inset). The low efficiency in the case of TrG3 is because of the agglomeration of particles (Fig. 12). The sheet-like structure was observed instead of nanoparticles that reduced the photon penetration power and act as shield for incoming photons (Nguyen-Phan et al. 2011). Hence, the photocatalytic degradation of BG decreased significantly for TrG3 nanocomposite material.

Table 1 BET surface area, pore volume (V_p), and pore size (D_p) of TiO₂ and TrG2 nanocomposite.

Sample	S_{BET} (m ² /g)	V_p (cm ³ /g)	D_p (nm)
TiO ₂	45.692	0.126	6.9
TrG2	65.698	0.182	13

Fig. 11 EIS analysis of as-synthesized TiO₂ and TrG2.

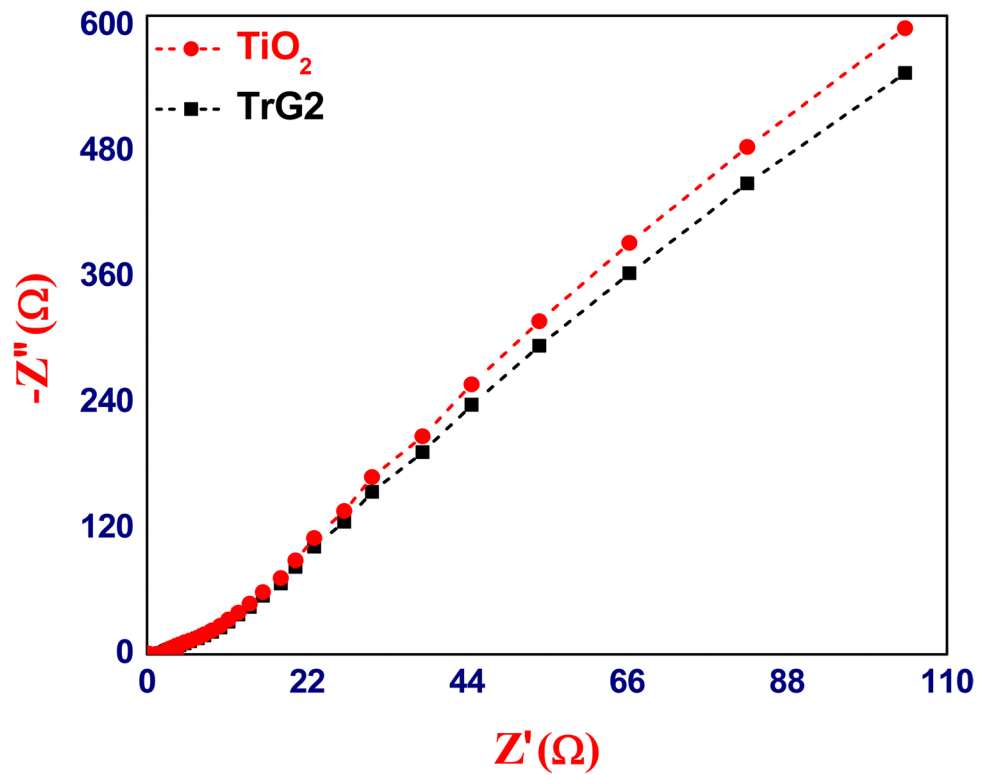


Fig. 12 Photocatalytic performance of the as-synthesized of as-synthesized TiO₂, TrG0.5, TrG1, TrG2, and TrG3. (inset; corresponding k_{app} values). Experimental conditions were the following: [BG]₀ = 10 mg.L⁻¹; catalyst amount = 10 mg/100 mL; radiation source = UV lamp (15W); pH = 6.35; irradiation time = 100 min.

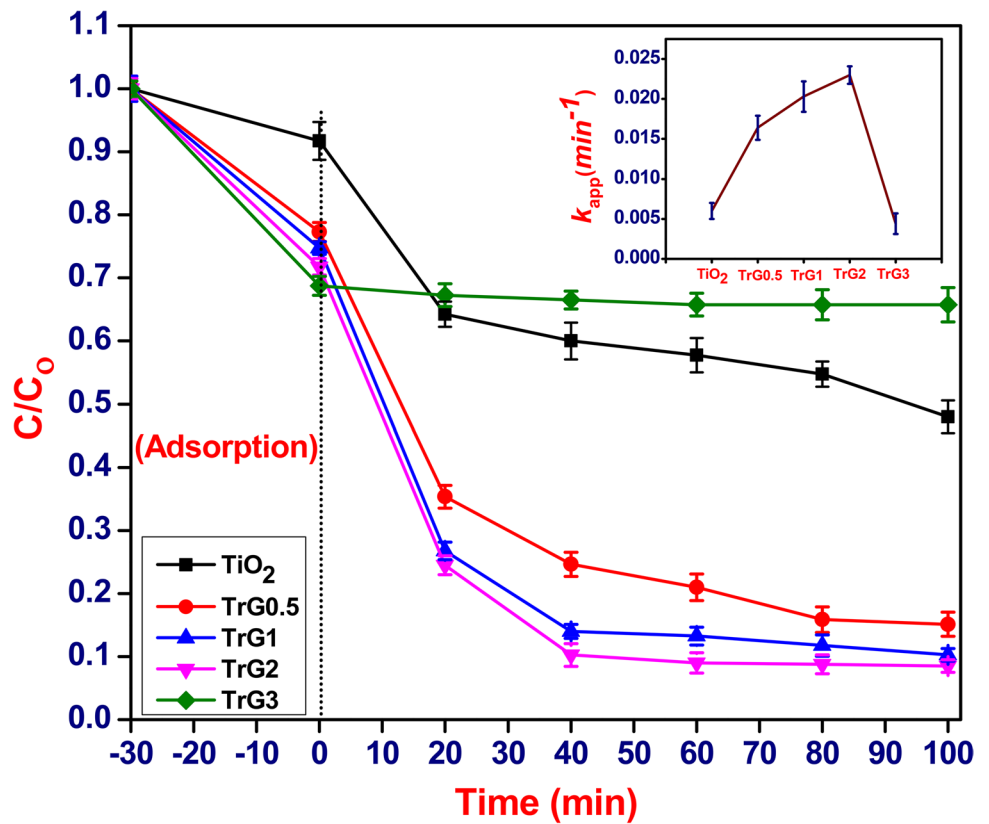


Figure S2 (supporting information) shows the degradation of BG in aqueous media by as-synthesized TrG2 under UV irradiations. The results revealed that after 80 min complete decolorization of dye has been achieved. Figures S3 and S4 (supporting information) show the corresponding visible spectra of BG degradation by TiO_2 and TrG2 respectively. In the case of TiO_2 , the decrease in absorbance occurred slowly, while in the case TrG2, this decrease in absorbance occurred very fast showing the high efficiency of TrG2 compared to TiO_2 .

Effects of operating factors in the photocatalytic efficiency of as-synthesized TrG2

Effect of initial amount of TrG2

Because of the high efficiency of TrG2 in terms of BG degradation compared to TiO_2 , TrG0.5, TrG1, TrG2, and TrG2, this composite material was selected for further degradation study. Once the best material was obtained, i.e., TrG2, then, the next step was to find its best amount. For this purpose, different amounts of the TrG2 (5, 10, 15, and 20 mg) were taken and the photocatalytic degradation of BG was performed under UV irradiations for 100 min. Figure 13 shows the effect of initial amount of TrG2 in BG degradation. It can be seen from the figure that by changing initial amount of TrG2 from 5 to 10 mg/100 mL, the photocatalytic activity was increased. The high efficiency for 10 mg

of as-synthesized TrG2 is due to the availability of large number of active sites that results in high adsorption of BG molecules over TrG2 surface (Tanhaei et al. 2015). Hence, the photocatalytic efficiency of TrG2 increases. However, further increase in initial amount of TrG2 from 10 to 20 mg decreases the photocatalytic efficiency for BG degradation under UV irradiations. This decrease in efficiency might be due to the shielding phenomenon that was observed in the case of high amount of TrG2 that decreases the photon penetration power to large extent hence (Augugliaro et al. 2006). The k_{app} values for various initial amount of TrG2 (5, 10, 15, and 20 mg) were obtained by applying *pseudo-first-order* kinetic equation on data (Fig. 13; inset). The data revealed that 10 mg of as-synthesized TrG2 possess high k_{app} value of 0.023 min^{-1} compared to 5, 15, and 20 mg of TrG2. Furthermore, it can be seen from Fig. 13 that the adsorption of BG over TrG2 surface increases regularly with increase in initial amount of TrG2 from 5 to 20 mg. The high adsorption in the case of 20 mg of TrG2 may be the availability of large number of active sites for BG adsorption.

Effect of peroxymonosulfate (PMS)

The photocatalytic efficiency of as-synthesized TrG2 toward BG degradation was also determined in the presence PMS in the reaction mixture. The $\text{SO}_4^{\bullet-}$ were introduced into the reaction mixture by means of PMS addition. The effect of initial concentration of PMS (0.1–2.0 mM)

Fig. 13 Effects of initial amount of as-synthesized TrG2 (5, 10, 15, and 20 mg) in terms of BG degradation in aqueous media. (inset; corresponding k_{app} values). Experimental conditions were the following: $[\text{BG}]_0 = 10 \text{ mg}\cdot\text{L}^{-1}$; irradiation source = UV lamp (15W); pH = 6.35; irradiation time = 100 min.

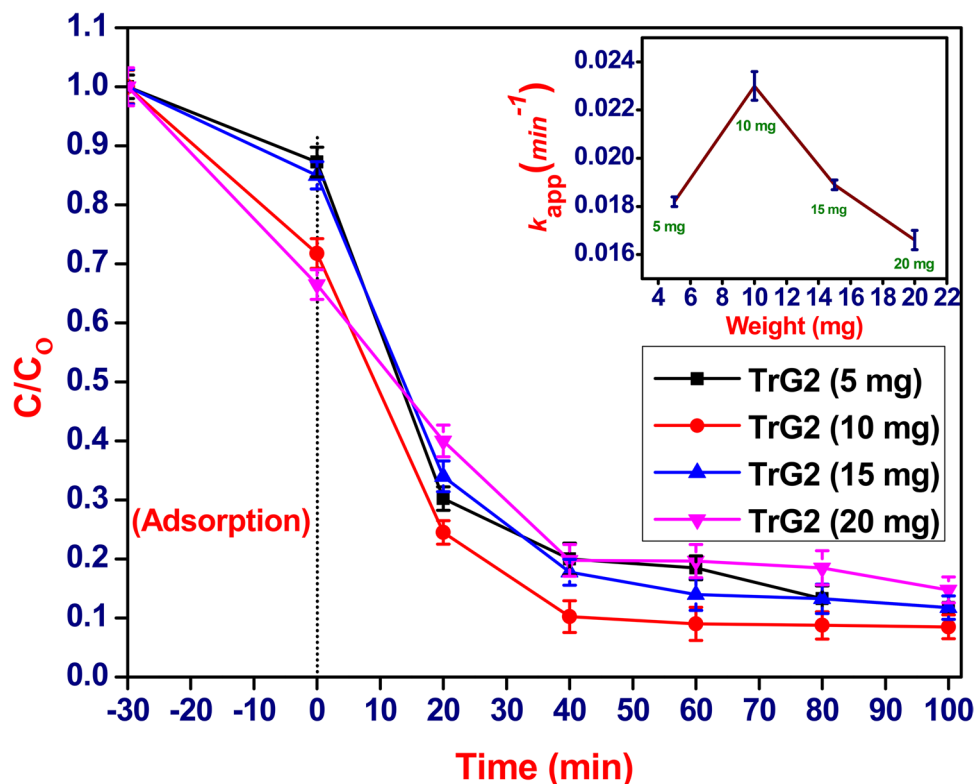
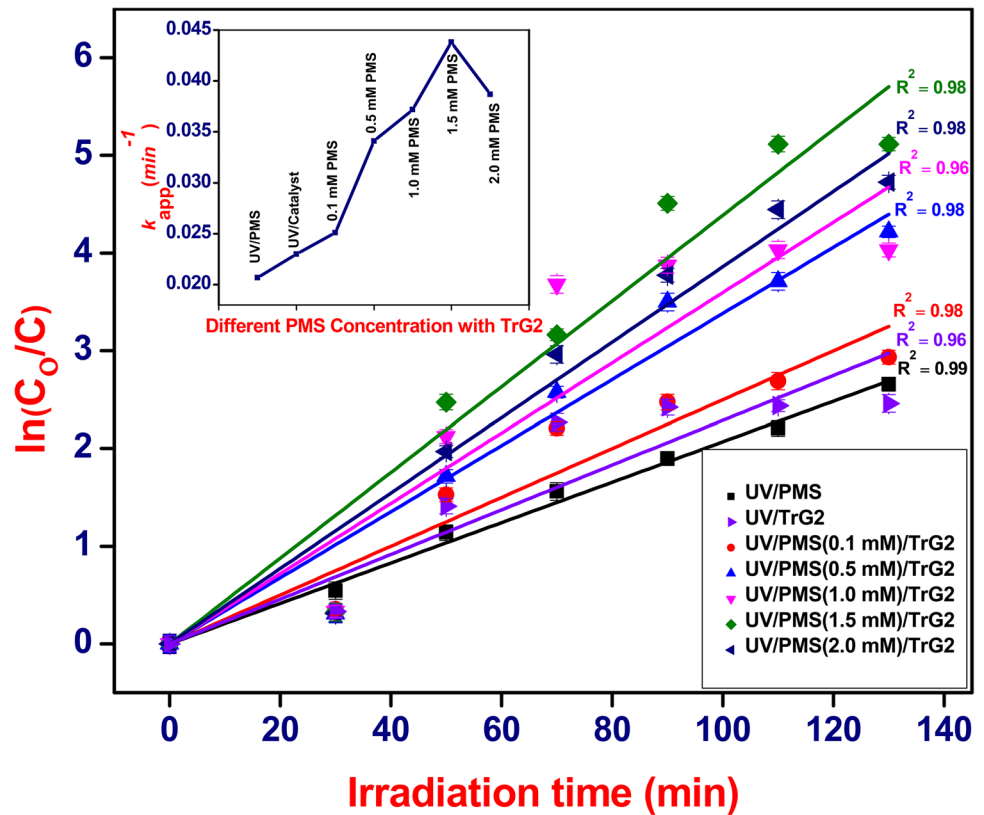
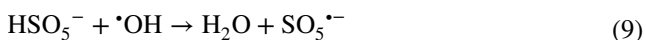
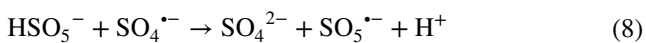


Fig. 14 Kinetic plots for BG by as-synthesized TrG2 with different PMS concentrations (inset; k_{app} values). Experimental conditions were the following: $[BG]_0 = 10 \text{ mg}\cdot\text{L}^{-1}$; catalyst amount = 10 mg/100 mL; PMS concentration (0.1–2.0 mM); irradiation source = UV lamp (15W); pH = 6.35; irradiation time = 100 min.



in BG degradation is shown in Fig. 14. It can be seen from Fig. 14 that by increasing the initial concentration of PMS from 0.1 to 1.5 mM the efficiency of the photocatalytic process increases and more than 90% degradation of BG was observed at a reaction time of 40 min (Rehman et al. 2018). The k_{app} values calculated by applying pseudo-first-order kinetic equation on data were 0.023, 0.0251, 0.0341, 0.0372, 0.0438, and 0.0387 min^{-1} for the initial concentration of PMS of 0.0, 0.1, 0.5, 1.0, 1.5, and 2.0 mM, respectively (Fig. 14; inset). High concentration of PMS enhanced the degradation of BG because of high concentration of $\text{SO}_4^{\bullet-}$ and $\bullet\text{OH}$ production (Zhang et al. 2022). However, further increase in PMS concentration after 1.5 mM showed no significant increase in rate of BG degradation instead the rate of degradation was decreased which might be due to the following two reasons; Penetration power of UV irradiations decreased upon further increase in concentration of PMS which decreased the formation of radical species and quenching of $\text{SO}_4^{\bullet-}$ and $\bullet\text{OH}$ by PMS in the case of high concentration (Eqs. 8, 9) (Shukla et al. 2010).



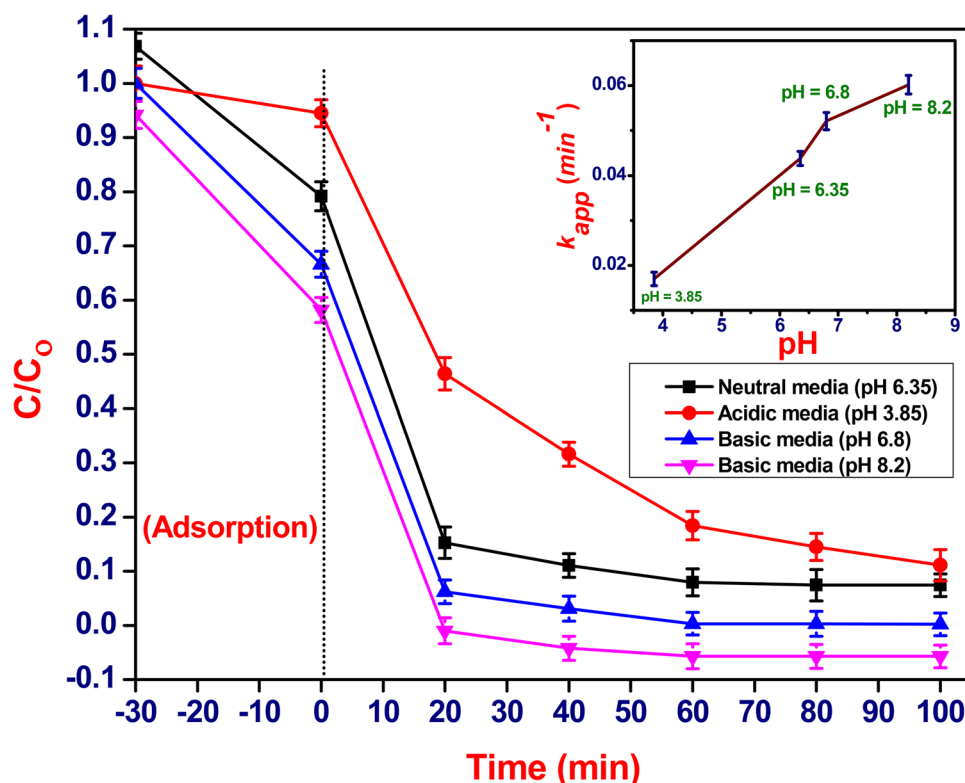
Effect of initial pH of the solution

pH of the medium play a key role in photocatalytic process because it affect the charge over the surface of catalyst, adsorption-desorption of contaminants over the catalyst surface and ionic state of the contaminant (Chekuri and Tirukkavalluri 2017). For this purpose degradation of BG was also carried out in various media i.e., neutral media, acidic media, and basic media in order to examine the efficiency of as-synthesized TrG2. For pH adjustment, HClO_4 and NaOH were utilized.

Figure 15 shows the degradation of BG by as-synthesized TrG2 aided PMS under UV irradiations in different media (acidic, neutral, and basic). The efficiency of TrG2 for BG degradation was in the order of the following: acidic < neutral < basic with the k_{app} values of 0.017, 0.0438, 0.0521, and 0.0602 min^{-1} (Fig. 15; inset) for pH 3.85, 6.35, 6.8, and 8.2 respectively. The low efficiency of BG degradation in acidic media may be due to the following reasons;

1. Upon the introduction of HClO_4 in aqueous media, the formation of H^+ occurred that react with the generated $\bullet\text{OH}$ to produce water molecules (Kim et al. 2021). As here the concentration of $\bullet\text{OH}$ decreases therefore, the rate of BG degradation decreases in acidic media.

Fig. 15 Photocatalytic performance of as-synthesized TrG2 in acidic, basic, and neutral media. (inset; corresponding k_{app} values). Experimental conditions were the following: $[BG]_0 = 10 \text{ mg}\cdot\text{L}^{-1}$; catalyst amount = 10 mg/100 mL; irradiation source = UV lamp (15W); pH = 3.85–8.2; irradiation time = 100 min.



- The $\text{}^+\text{H}$ produced in acidic media scavenge the $\text{SO}_4^{\bullet-}$ produced by the addition of PMS (Huang et al. 2009).



- Upon the introduction of $\text{}^+\text{H}$ in media the positive charge develop on catalyst surface which decreased the adsorption of BG (cationic dye) over the catalyst surface that in turn decreased the rate photocatalytic degradation of BG (Chen et al. 2008). The enhance degradation of BG was observed in basic media. The high rate of BG degradation in basic media may be due to the following reasons;

- Upon the addition of NaOH, the hydroxide ions ($\text{}^-\text{OH}$) were produced that reacts with the positively charged holes ($\text{}^+\text{h}$) in the material which results in $\cdot\text{OH}$ formation that in turn increased the rate of BG degradation (Chen et al. 2008).



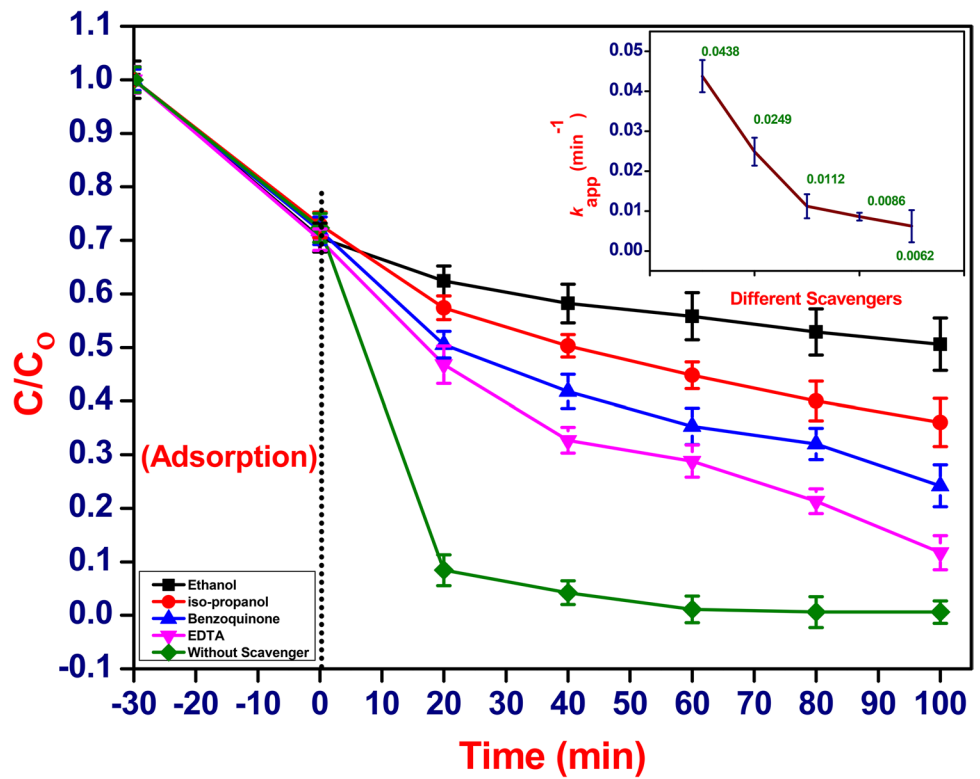
- High adsorption of BG over material surface as the pH of the medium was increased which results in high rate

of BG degradation which is in good agreement with our PZC results.

Effect of different radical scavengers

For determining the role of various active species ($\cdot\text{OH}$, $\text{SO}_4^{\bullet-}$, h^+ , and $\text{O}_2^{\bullet-}$) responsible for BG degradation, some scavenger experiments were performed using ethanol ($\cdot\text{OH}$, and $\text{SO}_4^{\bullet-}$ scavenger), isopropanol ($\cdot\text{OH}$ scavenger), benzoquinone ($\text{O}_2^{\bullet-}$ and O_2 scavenger) and EDTA (h^+ scavenger). Figure 16 shows the effects of various scavengers in the degradation of BG by as-synthesized TrG2 in aqueous media. The results revealed that in the presence of ethanol the percent degradation decreased from 99.4 to 49.4%. In the case of isopropanol, the percent degradation reached to 64%. For benzoquinone and EDTA the percent degradation was found to be 75.8 and 81.2% respectively. The rate of BG degradation followed the order of the following: without scavenger > EDTA > benzoquinone > isopropanol > ethanol (Fig. 16) with the k_{app} of 0.0438, 0.0249, 0.0112, 0.0086, and 0.0062 min^{-1} respectively (Fig. 16; inset). These results confirmed $\cdot\text{OH}$, and $\text{SO}_4^{\bullet-}$ as the main species responsible for BG degradation (Sayed et al. 2020). The visible spectra of BG degradation in the presence of benzoquinone,

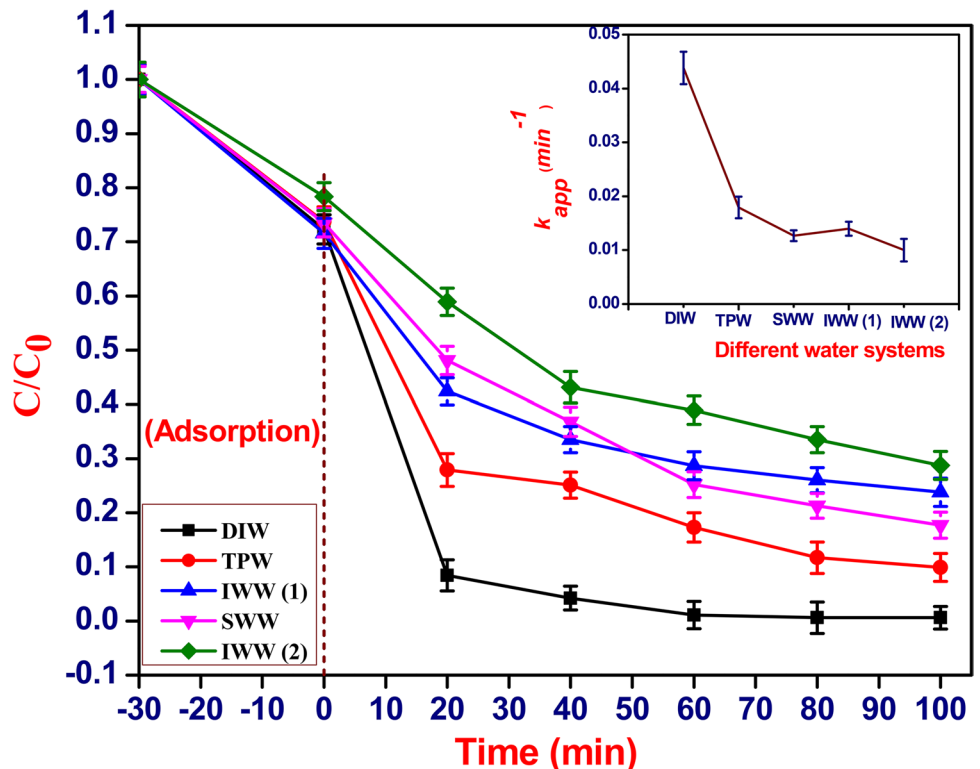
Fig. 16 Role of scavengers in photocatalytic performance of as-synthesized TrG2 for BG degradation under UV irradiation. (inset; corresponding k_{app} values). Experimental conditions were the following: $[BG]_0 = 10 \text{ mg.L}^{-1}$; catalyst amount = 10 mg/100 mL; PMS concentration = 1.5 mM; radiation source = UV lamp (15W); pH = 6.35; irradiation time = 100 min.



isopropanol, and ethanol are depicted in Fig. S5(C) (supporting information) which shows that in the presence of ethanol the absorbance value decreased very slowly

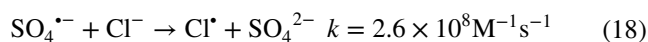
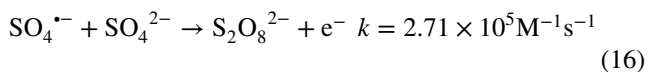
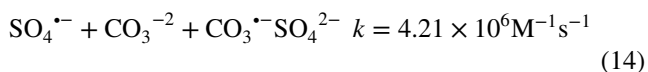
that confirmed its high scavenging ability for sulfate and hydroxyl radicals compared to isopropanol and benzoquinone.

Fig. 17 Photocatalytic performance of as-synthesized TrG2 in various water systems (inset; corresponding k_{app} values). Experimental conditions were the following: $[BG]_0 = 10 \text{ mg.L}^{-1}$; catalyst amount = 10 mg/100 mL; PMS concentration = 1.5 mM; radiation source = UV lamp (15W); irradiation time = 100 min.



Effect of different water systems

The efficiency of as-synthesized TrG2 for BG degradation was also examined in tap water, synthetic wastewater, and BG-contaminated industrial wastewater besides distilled water. Figure 17 shows the photocatalytic degradation of BG by TrG2 added PMS in different water systems. The efficiency of TrG2 for BG removal followed the order of the following: distilled water (DIW) > tap water (TPW) > industrial wastewater 1 (IWW (1)) > synthetic wastewater (SWW) > industrial wastewater 2 (IWW (2)) with the k_{app} of 0.0438, 0.0176, 0.0127, 0.014, and 0.010 min^{-1} respectively (Fig. 17; inset). The decreased rate of BG degradation in the case of TPW is due to the presence of small amount of dissolved carbonate (CO_3^{2-}), sulfate (SO_4^{2-}), and chloride (Cl^-) ions that acts as scavengers for $\bullet\text{OH}$ and $\text{SO}_4^{\bullet-}$ (Rehman et al. 2021).

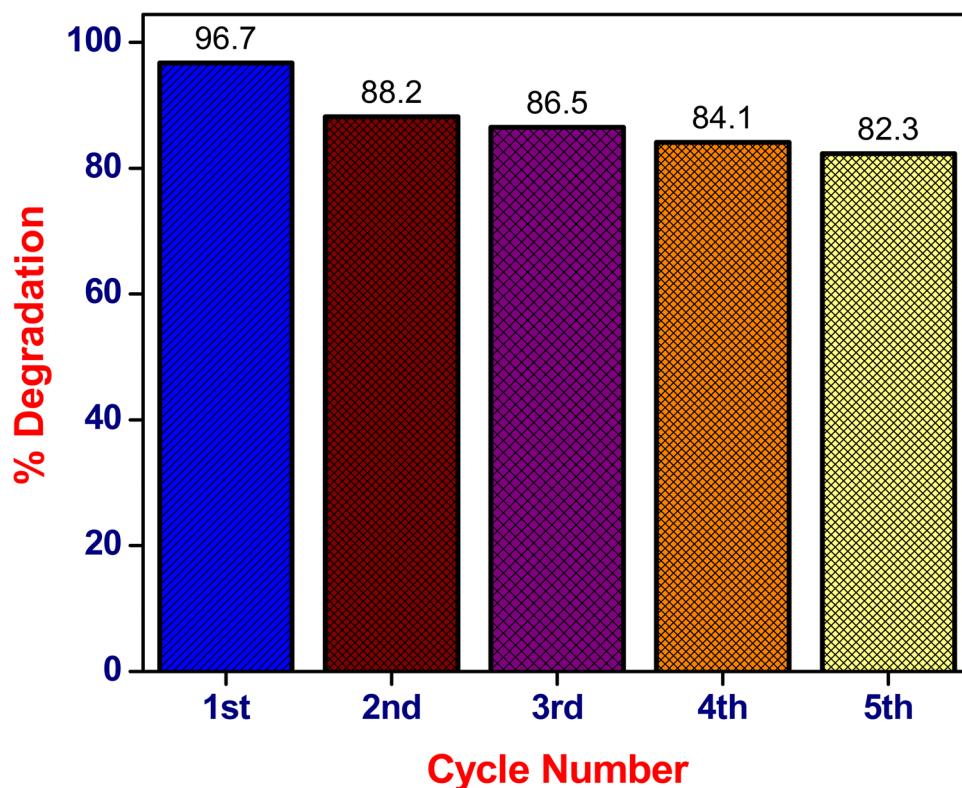


The low percent degradation of BG (76.2%) in the case of SWW is because of the high concentration of $\text{FeSO}_4 \cdot 7\text{H}_2\text{O}$ (2 mg/100 mL), NaHCO_2 (22 mg/100 mL), NaCl (2 mg/100 mL), $\text{MgSO}_4 \cdot 7\text{H}_2\text{O}$ (1.5 mg/100 mL), CaCl_2 (1 mg/100 mL), NH_4Cl (5 mg/100 mL), and EDTA (2 mg/100 mL) (Pelaez et al. 2011). In the case of IWW (1), 82.3% degradation of BG was observed that might be due to the very high concentration of NaCl compared to DIW and SWW. In the case of IWW (2), the percent degradation reached to 60% that could be attributed to different types of contaminants (salts, alcohols, dyes) beside BG dye that are present in IWW (2) sample (Chakrabarti and Dutta 2004).

Photocatalytic stability of as-synthesized TrG2

The most important characteristic of the photocatalyst is its reusability toward the elimination of the targeted contaminants. For determining the photocatalytic stability of the as-synthesized TrG2, the recycling experiments were performed. At the end of each experiment the TrG2 nanocomposites were recovered by the process of centrifugation (7000 rpm). The recovered nanocomposites were washed

Fig. 18 Recycling experiments showing the photocatalytic performance of as-synthesized TrG2 toward BG degradation after each cycle in aqueous media. Experimental conditions were the following: $[\text{BG}]_0 = 10 \text{ mg} \cdot \text{L}^{-1}$; catalyst amount = 50 mg/100 mL; PMS concentration = 1.5 mM; radiation source = UV lamp (15W); irradiation time = 100 min.



away numerous times with ethanol and distilled water followed by vacuum dryness in an oven at a temperature of 80°C for 5 h. After dryness, the sample was used for 2nd, 3rd, 4th, and 5th cycles respectively by applying the same procedure. Figure 18 shows the high stability of the as-synthesized TrG2 material. It can be seen from Fig. 18 that up to 5th cycle the TrG2 material showed good response toward BG degradation (more than 80% of BG removal). Besides, the percent degradation of BG by as-synthesized TrG2 decreases from 96.7 to 82.3% at the end of 5th cycle that might be due to the loss of catalyst material during the recovery process. The weight loss of TrG2 material after each experiment could be one of the possible reasons. (Abdi et al. 2020). The second possible reason of low catalytic activity may be due to the poisoning of catalyst material by BG by-products that results in its low photocatalytic activity (Chan et al. 2020).

Mechanism of photocatalytic degradation of BG by as-synthesized TrG2 added PMS system (TrG2/PMS)

The proposed mechanism of photocatalysis is expected to be as follows;

In TrG2 the valence band (VB) and conduction band (CB) of TiO₂ are positioned at 2.96 and -0.16 respectively (Fig. 19) (supporting information; S6). Upon irradiating the TiO₂ surface with UV irradiations, the electrons transfer from its VB to the CB. As a result of this electrons transfer holes are generated in the VB. (Kumar et al. 2015). The excited electrons in the CB of TiO₂ migrate toward the newly

formed rGO sheets lying near the CB of TiO₂ (Fujisawa et al. 2017). The as-synthesized rGO act as electron sink or electron reservoir for these photogenerated electrons (Xu et al. 2018). Hence the problem of electron-hole pair recombination became solved effectively by the incorporation of rGO in TiO₂ system. The photogenerated electrons from the rGO sheet attack the peroxymonosulfate molecules (PMS) and produce the highly reactive SO₄^{•-} and [•]OH (Antoniou et al. 2018). On the other hand, the (h⁺) that are produced in the VB band of TiO₂ upon UV irradiations attack the H₂O molecules and cause the formation of [•]OH (Ghaly et al. 2011). Besides, the PMS is also get activated by UV irradiations to produce SO₄^{•-} and [•]OH. All these generated radicals (SO₄^{•-} and [•]OH) directly attack the BG molecules and cause its degradation followed by mineralization (formation of CO₂ and H₂O) (Fig. 19).

By-product analysis and proposed degradation pathways

For by-product analysis, the photocatalytic degradation of BG was performed in TrG2 added PMS system under UV irradiation for 100 min. GC-MS analysis was carried out for qualitative determination of degraded by-products. The GC-MS results of BG indicate five degradation products (DPs) that were formed during the photocatalytic process due to the attack of SO₄^{•-} and/or [•]OH on BG dye. The detail of these DPs is summarized in Table 2. The possible degradation pathways of BG are also depicted in Fig. 20 accordingly. The main mechanisms by which SO₄^{•-} and/or [•]OH attack BG are addition to unsaturated bonds, elimination,

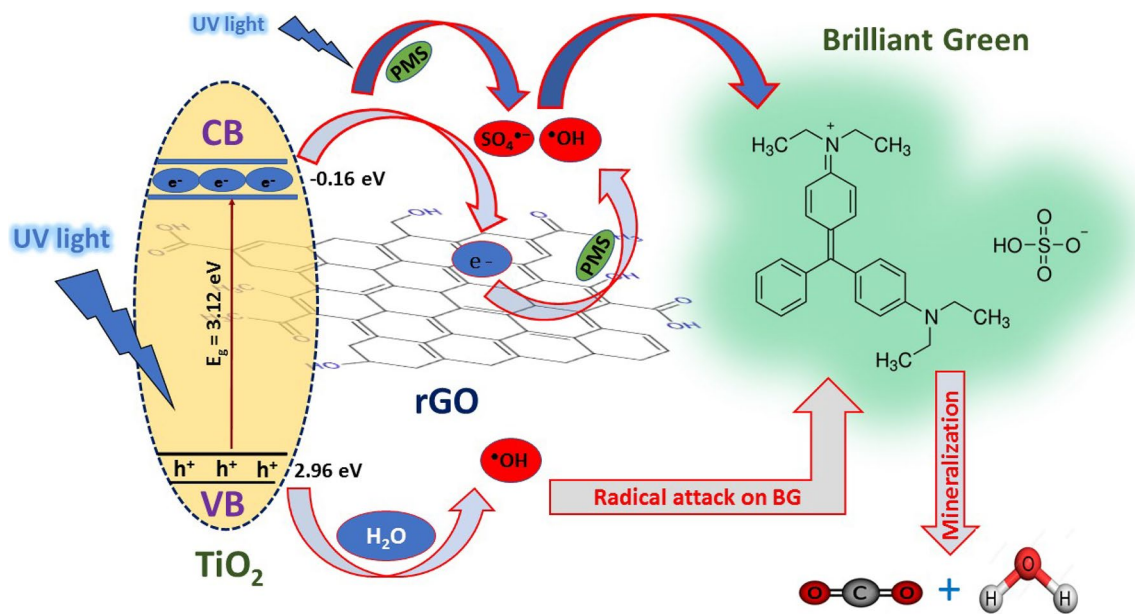
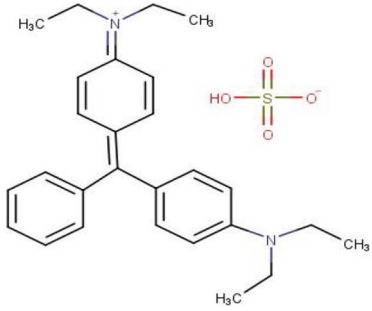
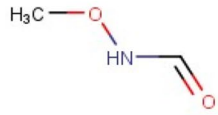
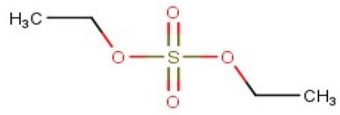
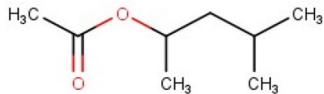
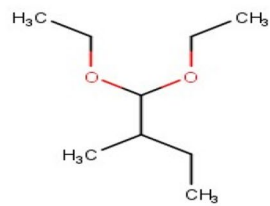
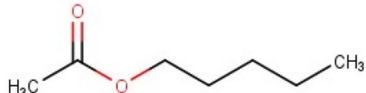


Fig. 19 Proposed mechanism for the photocatalytic degradation of BG by as-synthesized TrG2 added PMS system.

Table 2 Details of by-products produced during the photocatalytic degradation of BG by as-synthesized TrG2 added PMS system (TrG2/PMS)

S.No	Chemical Structure	Chemical Formula	Abbreviated Form	m/z value
1		C ₂₇ H ₃₄ N ₂ O ₄ S	BG	475.6
2		C ₂ H ₅ NO ₂	DP1	75.07
3		C ₄ H ₁₀ O ₄ S	DP2	154.19
4		C ₈ H ₁₆ O ₂	DP3	144.2
5		C ₉ H ₂₀ O ₂	DP4	160.25
6		C ₇ H ₁₄ O ₂	DP5	130.18

hydrogen abstraction, and processes involving the transfer of electrons and substitution. $\text{SO}_4^{\bullet-}$ frequently attacks using an electron transfer mechanism and $\bullet\text{OH}$ frequently attacks via hydrogen abstraction and addition processes (Gul et al. 2021). Figure 20 shows that the production of DP1 ($m/z = 75.07$) could be due to the detachment of one of the nitrogen segments of BG at “N” position, which may possibly be attributed to $\bullet\text{OH}$ or $\text{SO}_4^{\bullet-}$ attack. The degradation product

DP2 ($m/z = 154.19$) is mainly resulted from HSO_4^- of BG, where one ethyl group became attached to each singly bonded oxygen atom. This HSO_4^- group of BG is basically a counter ion for the cationic portion of BG. The formation of DP3 ($m/z = 144$) is due to the ring opening of BG at various positions that might be due to the attack of $\bullet\text{OH}$ and/or $\text{SO}_4^{\bullet-}$. The degradation product DP4 ($m/z = 160.25$) and DP5 ($m/z = 130.18$) might be attributed to $\bullet\text{OH}$ and/or

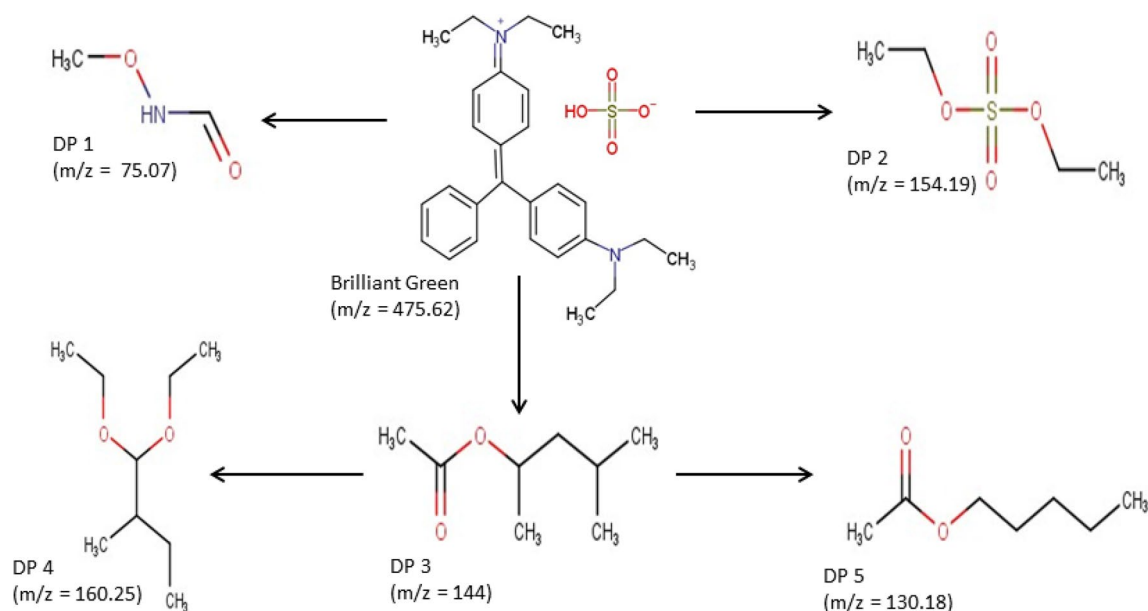


Fig. 20 Proposed pathways of BG degradation by as-synthesized TrG2 in the presence of PMS.

$\text{SO}_4^{\bullet-}$ attack on DP3. It can be seen that these degradation products (DP4 and DP5) could be produced due to the rearrangement, addition, and removal of some groups in DP3.

Conclusions

In this study, the light responsive titania/reduced graphene oxide nanocomposites (TiO_2/rGO) were synthesized by simple hydrothermal method by changing the concentration of graphene oxide (GO) while the concentration of TiO_2 was kept constant. Different techniques (SEM, TEM, HRTEM, XRD, EDX, TGA, UV-DRS, PL, EIS, and BET) were used for the characterization of as-synthesized rGO, TiO_2 , and TiO_2/rGO that revealed the high crystallinity, small crystallite size (18.4 nm), high thermal stability, low band gap energy (3.12 eV), and decrease electron-hole pair recombination for as-synthesized TiO_2/rGO . The efficiency of as-synthesized TiO_2 and TiO_2/rGO nanocomposites were determined in terms of BG degradation under UV irradiations. The results revealed that TrG2 (2% composite material) showed high efficiency for BG removal i.e., more than 90% degradation was achieved within 60 min of time with the k_{app} of 0.023 min^{-1} . The rate of BG degradation was further improved by the incorporation of PMS in aqueous media. The pH experiments showed the high performance of as-synthesized TrG2 in basic media. Furthermore, the radicals scavenging experiments revealed $\bullet\text{OH}$ and $\text{SO}_4^{\bullet-}$ as the major species involved in BG degradation under UV irradiations. Besides, the degradation

of BG by as-synthesized TrG2 added PMS was also performed in different water matrices that revealed the high efficiency of TrG2 for BG degradation. Thus, the proposed UV/TrG2/PMS system can be a novel perspective for the effective removal of contaminants from aqueous media.

Supplementary Information The online version contains supplementary material available at <https://doi.org/10.1007/s11356-023-27316-3>.

Acknowledgements The authors are highly thankful to the Higher Education Commission (HEC) of Pakistan for funding this research project. Moreover, the authors extend their appreciation to the National Centre of Excellence in Physical Chemistry, University of Peshawar, Pakistan for providing research facilities. Authors are also thankful to Ms. Sadia Rehman of School of Environment, Tsinghua University, Beijing, China, for BET analysis.

Author contribution The individual contributions by all the authors to this paper can be summarized below: Qaiser Khan: conceptualization; data curation; formal analysis; investigation; methodology; original draft writing. Murtaza Sayed: project administration; supervision; funding acquisition. Ikhtiar Gul: formal analysis; investigation; validation; editing.

Data availability The data and materials that support the findings of this study are openly available on request.

Declarations

Ethical approval Not applicable.

Consent to participate Not applicable.

Consent for publication Not applicable.

Competing interests The authors declare no competing interests.

References

- Abdel Rahman RO, Hung Y-T (2020) Application of ionizing radiation in wastewater treatment: an overview. *Water* 12(1):19
- Abdi M, Mahdikah V, Sheibani S (2020) Visible light photocatalytic performance of La-Fe co-doped SrTiO₃ perovskite powder. *Opt Mater* 102:109803
- Ambrosi A, Chua CK, Khezri B, Sofer Z, Webster RD, Pumera M (2012) Chemically reduced graphene contains inherent metallic impurities present in parent natural and synthetic graphite. *Proc Natl Acad Sci* 109(32):12899–12904
- Ameta R, Solanki MS, Benjamin S, Ameta SC (2018) Photocatalysis. In: *Advanced oxidation processes for waste water treatment*. Academic Press, pp 135–175
- Antoniou MG, Boraei I, Solakidou M, Deligiannakis Y, Abhishek M, Lawton L, Edwards C (2018) Enhancing photocatalytic degradation of the cyanotoxin microcystin-LR with the addition of sulfate-radical generating oxidants. *J Hazard Mater* 360:461–470
- Arslan I, Balcioglu IA, Tuhkanen T (1999) Advanced oxidation of synthetic dyehouse effluent by O₃, H₂O₂/O₃ and H₂O₂/UV processes. *Environ Technol* 20(9):921–931
- Augugliaro V, Litter M, Palmisano L, Soria J (2006) The combination of heterogeneous photocatalysis with chemical and physical operations: a tool for improving the photoprocess performance. *J Photochem Photobiol C Photochem Rev* 7(4):127–144
- Bakatula EN, Richard D, Neculita CM, Zagury GJ (2018) Determination of point of zero charge of natural organic materials. *Environ Sci Pollut Res* 25(8):7823–7833
- Balsamo SA, Fiorenza R, Condorelli M, Pecoraro R, Brundo MV, Lo Presti F, Sciré S (2021) One-pot synthesis of TiO₂-rGO photocatalysts for the degradation of groundwater pollutants. *Materials* 14(20):5938
- Chakrabarti S, Dutta BK (2004) Photocatalytic degradation of model textile dyes in wastewater using ZnO as semiconductor catalyst. *J Hazard Mater* 112(3):269–278
- Chan K-L, Lin W-H, Chen F-J, Yang M-H, Jiang C-H, Lee C-Y, Lee C-Y (2020) Photocatalytic performance of bipyramidal anatase TiO₂ toward the degradation organic dyes and its catalyst poisoning effect. *React Kinet Mech Catal* 130:531–546
- Chekuri RD, Tirukkavalluri SR (2017) Synthesis of cobalt doped titania nano material assisted by gemini surfactant: characterization and application in degradation of Acid Red under visible light irradiation. *SAJCE* 24(1):183–195
- Chen C-C, Lu C-S, Fan H-J, Chung W-H, Jan J-L, Lin H-D, Lin W-Y (2008) Photocatalyzed N-de-ethylation and degradation of Brilliant Green in TiO₂ dispersions under UV irradiation. *Desalination* 219(1-3):89–100
- Chen M, Meng Y, Zhang W, Zhou J, Xie J, Diao G (2013) β-Cyclodextrin polymer functionalized reduced-graphene oxide: application for electrochemical determination imidacloprid. *Electrochim Acta* 108:1–9
- Collazzo G, Jahn S, Carreño N, Foletto E (2011) Temperature and reaction time effects on the structural properties of titanium dioxide nanopowders obtained via the hydrothermal method. *Braz J Chem Eng* 28:265–272
- Dong Z, Zondag SD, Schmid M, Wen Z, Noël T (2022) A meso-scale ultrasonic milli-reactor enables gas–liquid–solid photocatalytic reactions in flow. *Chem Eng J* 428:130968
- Fujisawa J-I, Eda T, Hanaya M (2017) Comparative study of conduction-band and valence-band edges of TiO₂, SrTiO₃, and BaTiO₃ by ionization potential measurements. *Chem Phys Lett* 685:23–26
- Gavgani JN, Adelnia H, Gudarzi MM (2014) Intumescent flame retardant polyurethane/reduced graphene oxide composites with improved mechanical, thermal, and barrier properties. *J Mater Sci* 49(1):243–254
- Ghaly MY, Jamil TS, El-Seesy IE, Souaya ER, Nasr RA (2011) Treatment of highly polluted paper mill wastewater by solar photocatalytic oxidation with synthesized nano TiO₂. *Chem Eng J* 168(1):446–454
- Gul I, Sayed M, Shah NS, Khan JA, Polychronopoulou K, Iqbal J, Rehman F (2020) Solar light responsive bismuth doped titania with Ti³⁺ for efficient photocatalytic degradation of flumequine: Synergistic role of peroxymonosulfate. *Chem Eng J* 384:123255
- Gul I, Sayed M, Shah NS, Rehman F, Khan JA, Gul S, Iqbal J (2021) A novel route for catalytic activation of peroxymonosulfate by oxygen vacancies improved bismuth-doped titania for the removal of recalcitrant organic contaminant. *Environ Sci Pollut Res* 28(18):23368–23385
- Gupta B, Melvin AA (2017) TiO₂/RGO composites: its achievement and factors involved in hydrogen production. *Renew Sustain Energy Rev* 76:1384–1392
- Hanifah MFR, Jaafar J, Othman M, Ismail A, Rahman MA, Yusof N, Aziz F (2019) Facile synthesis of highly favorable graphene oxide: effect of oxidation degree on the structural, morphological, thermal and electrochemical properties. *Materialia* 6:100344
- Hu J, He B, Lu J, Hong L, Yuan J, Song J, Niu L (2012) Facile preparation of pt/polyallylamine/reduced graphene oxide composites and their application in the electrochemical catalysis on methanol oxidation. *Int J Electrochem Sci* 7(10):10094–10107
- Huang, Y.-H., Huang, Y.-F., Huang, C.-i., & Chen, C.-Y. (2009). Efficient decolorization of azo dye Reactive Black B involving aromatic fragment degradation in buffered Co²⁺/PMS oxidative processes with a ppb level dosage of Co²⁺-catalyst. *J Hazard Mater*, 170(2-3), 1110-1118.
- Irshad MA, Nawaz R, ur Rehman, M. Z., Imran, M., Ahmad, J., Ahmad, S., Ali, S. (2020) Synthesis and characterization of titanium dioxide nanoparticles by chemical and green methods and their antifungal activities against wheat rust. *Chemosphere* 258:127352
- Jian Y, Liu H, Zhu J, Zeng Y, Liu Z, Hou C, Pu S (2021) Preparation of F-doped H₂ Ti₃O₇-{104} nanorods with oxygen vacancies using TiOF₂ as precursor and its photocatalytic degradation activity. *RSC Adv* 11(56):35215–35227
- Khan JA, He X, Shah NS, Sayed M, Khan HM, Dionysiou DD (2017) Degradation kinetics and mechanism of desethyl-atrazine and desisopropyl-atrazine in water with OH and SO₄⁻ based-AOPs. *Chem Eng J* 325:485–494
- Khan S, Sayed M, Sohail M, Shah LA, Raja MA (2019) Advanced oxidation and reduction processes. In: *Advances in water purification techniques*, pp 135–164
- Khavar AHC, Moussavi G, Mahjoub AR (2018) The preparation of TiO₂@rGO nanocomposite efficiently activated with UVA/LED and H₂O₂ for high rate oxidation of acetaminophen: catalyst characterization and acetaminophen degradation and mineralization. *Appl Surf Sci* 440:963–973
- Kim YK, Rousseau R, Kay BD, White J, Dohnálek Z (2008) Catalytic dehydration of 2-propanol on (WO₃)₃ clusters on TiO₂ (110). *J Am Chem Soc* 130(15):5059–5061
- Kim MS, Lee C, Kim JH (2021) Occurrence of unknown reactive species in UV/H₂O₂ system leading to false interpretation of hydroxyl radical probe reactions. *Water Res* 201:117338
- Kovačić M, Perović K, Papac J, Tomić A, Matoh L, Žener B, Kušić H (2020) One-pot synthesis of sulfur-doped TiO₂/reduced graphene oxide composite (S-TiO₂/rGO) with improved photocatalytic activity for the removal of diclofenac from water. *Materials* 13(7):1621
- Kumar R, Rashid J, Barakat M (2015) Zero valent Ag deposited TiO₂ for the efficient photocatalysis of methylene blue under UV-C light irradiation. *Colloids and Interface Science Communications* 5:1–4

- Le TT, Tran TD (2020) Photocatalytic degradation of rhodamine B by C and N codoped TiO₂ nanoparticles under visible-light irradiation. *J Chem*. <https://doi.org/10.1155/2020/4310513>
- Li H, Ren F, Liu J, Wang Q, Li Q, Yang J, Wang Y (2015) Endowing single-electron-trapped oxygen vacancy self-modified titanium dioxide with visible-light photocatalytic activity by grafting Fe (III) nanocluster. *Appl Catal Environ* 172:37–45
- Mansingh S, Sahoo DP, Paramanik L, Sahoo M, Parida K (2022) Robust charge carrier engineering via plasmonic effect and conjugated Π -framework on Au loaded ZnCr-LDH/RGO photocatalyst towards H₂ and H₂O₂ production. *Inorg Chem Front* 9(3):559–576
- Nada AA, Tantawy HR, Elsayed MA, Bechelany M, Elmowafy ME (2018) Elaboration of nano titania-magnetic reduced graphene oxide for degradation of tartrazine dye in aqueous solution. *Solid State Sci* 78:116–125
- Nainani RK, Thakur P (2016) Facile synthesis of TiO₂-RGO composite with enhanced performance for the photocatalytic mineralization of organic pollutants. *Water Sci Technol* 73(8):1927–1936
- Nassar I (2019) *Continuous flow photodegradation of olive Zebur contaminants with simulated solar light using supported ZnO nanoparticles*, MSc Thesis. An-Najah National University, Nablus, Palestine
- Nguyen-Phan T-D, Pham VH, Shin EW, Pham H-D, Kim S, Chung JS, Hur SH (2011) The role of graphene oxide content on the adsorption-enhanced photocatalysis of titanium dioxide/graphene oxide composites. *Chem Eng J* 170(1):226–232
- Ouedraogo S, Chouchene B, Gries T, Desmarests C, Balan L, Gaumet J-J, Schneider R (2022) Bismuth oxybromide/reduced graphene oxide heterostructure sensitized with Zn-tetracarboxyphthalocyanine as a highly efficient photocatalyst for the degradation of Orange II and phenol. *J Environ Chem Eng* 10(2):107332
- Pei F, Xu S, Zuo W, Zhang Z, Liu Y, Cao S (2014) Effective improvement of photocatalytic hydrogen evolution via a facile in-situ solvothermal N-doping strategy in N-TiO₂/N-graphene nanocomposite. *Int J Hydrogen Energy* 39(13):6845–6852
- Pelaez M, Armah A, O’Shea K, Falaras P, Dionysiou DD (2011) Effects of water parameters on the degradation of microcystin-LR under visible light-activated TiO₂ photocatalyst. *Water Res* 45(12):3787–3796
- Pichon A, Lazuen-Garay A, James SL (2006) Solvent-free synthesis of a microporous metal-organic framework. *CrystEngComm* 8(3):211–214
- Preetha S, Pillai R, Ramamoorthy S, Mayeen A, Archana K, Kalarikkal N, Lekshmi I (2022) TiO₂-rGO nanocomposites with high rGO content and luminescence quenching through green redox synthesis. *Surf Interfaces* 30:101812
- Qi K, Cheng B, Yu J, Ho W (2017) Review on the improvement of the photocatalytic and antibacterial activities of ZnO. *J Alloys Compd* 727:792–820
- Rahman M, Tang Y, Kwong P (2018) Reduced recombination and low-resistive transport of electrons for photo-redox reactions in metal-free hybrid photocatalyst. *Appl Phys Lett* 112(25):253902
- Rehman F, Sayed M, Khan JA, Shah NS, Khan HM, Dionysiou DD (2018) Oxidative removal of brilliant green by UV/S₂O₈²⁻, UV/HSO₅⁻ and UV/H₂O₂ processes in aqueous media: a comparative study. *J Hazard Mater* 357:506–514
- Rehman F, Ahmad W, Sayed M (2021) Mechanistic investigations on the removal of diclofenac sodium by UV/S₂O₈²⁻/Fe²⁺, UV/HSO₅⁻/Fe²⁺ and UV/H₂O₂/Fe²⁺-based advanced oxidation processes. *Environ Technol* 42(25):3995–4005
- Sayed M, Khan A, Rauf S, Shah NS, Rehman F, Al-Kahtani A, A., Gul, I. (2020) Bismuth-doped nano zerovalent iron: a novel catalyst for chloramphenicol degradation and hydrogen production. *ACS omega* 5(47):30610–30624
- Sher Shah MSA, Park AR, Zhang K, Park JH, Yoo PJ (2012) Green synthesis of biphasic TiO₂-reduced graphene oxide nanocomposites with highly enhanced photocatalytic activity. *ACS Appl Mater Interfaces* 4(8):3893–3901
- Shukla P, Fatimah I, Wang S, Ang H, Tadé MO (2010) Photocatalytic generation of sulphate and hydroxyl radicals using zinc oxide under low-power UV to oxidise phenolic contaminants in wastewater. *Catalysis Today* 157(1-4):410–414
- Simon T, Carlson MT, Stolarczyk JK, Feldmann J (2016) Electron transfer rate vs recombination losses in photocatalytic H₂ generation on Pt-decorated CdS nanorods. *ACS energy letters* 1(6):1137–1142
- Sood S, Umar A, Mehta SK, Sinha A, Kansal SK (2015) Efficient photocatalytic degradation of brilliant green using Sr-doped TiO₂ nanoparticles. *Ceram Int* 41(3):3533–3540
- Sun L, Yan M, Xiao L, Liu Y, Bai H, Xie L, Shi W (2018) Synthesis of C/Co₃O₄ composite mesoporous hollow sphere sandwich graphene films for high-performance supercapacitors. *Inorg Chem Front* 5(10):2554–2562
- Szczepanik B (2017) Photocatalytic degradation of organic contaminants over clay-TiO₂ nanocomposites: a review. *Applied Clay Science* 141:227–239
- Tanhaei B, Ayati A, Lahtinen M, Sillanpää M (2015) Preparation and characterization of a novel chitosan/Al₂O₃/magnetite nanoparticles composite adsorbent for kinetic, thermodynamic and isotherm studies of Methyl Orange adsorption. *Chem Eng J* 259:1–10
- Tian L, Yang X, Liu Q, Qu F, Tang H (2018) Anchoring metal-organic framework nanoparticles on graphitic carbon nitrides for solar-driven photocatalytic hydrogen evolution. *Appl Surf Sci* 455:403–409
- Tolosana-Moranchel A, Casas J, Bahamonde A, Pascual L, Granone L, Schneider J, Bahnemann D (2019a) Nature and photoreactivity of TiO₂-rGO nanocomposites in aqueous suspensions under UV-A irradiation. *Appl Catal Environ* 241:375–384
- Tolosana-Moranchel A, Manassero A, Satuf ML, Alfano OM, Casas JA, Bahamonde A (2019b) Influence of TiO₂-rGO optical properties on the photocatalytic activity and efficiency to photodegrade an emerging pollutant. *Appl Catal Environ* 246:1–11
- Trojanowicz M, Bobrowski K, Szreder T, Bojanowska-Czajka A (2018) Gamma-ray, X-ray and electron beam based processes. In: *Advanced oxidation processes for waste water treatment*. Academic Press, pp 257–331
- Viet TQQ, Nhu TH, Trinh DN, Giang NTH, Dat NM, Hieu NH (2021) Optimization of TiO₂ immobilized-reduce graphene oxide photocatalyst toward organic compounds in aqueous medium. *Synth Met* 280:116867
- Wang JL, Xu LJ (2012) Advanced oxidation processes for wastewater treatment: formation of hydroxyl radical and application. *Crit Rev Environ Sci Technol* 42(3):251–325
- Wang P, Wang J, Wang X, Yu H, Yu J, Lei M, Wang Y (2013) One-step synthesis of easy-recycling TiO₂-rGO nanocomposite photocatalysts with enhanced photocatalytic activity. *Appl Catal Environ* 132:452–459
- Xu D, Li L, He R, Qi L, Zhang L, Cheng B (2018) Noble metal-free RGO/TiO₂ composite nanofiber with enhanced photocatalytic H₂-production performance. *Appl Surf Sci* 434:620–625
- Yu C, Tan L, Shen S, Fang M, Yang L, Fu X, Sun J (2021) In situ preparation of g-C₃N₄/polyaniline hybrid composites with enhanced visible-light photocatalytic performance. *J Environ Sci* 104:317–325
- Zhang X, Liu Y, Li C, Tian L, Yuan F, Zheng S, Sun Z (2022) Fast and lasting electron transfer between γ -FeOOH and g-C₃N₄/kaolinite containing N vacancies for enhanced visible-light-assisted peroxymonosulfate activation. *Chem Eng J* 429:132374

Publisher's note Springer Nature remains neutral with regard to jurisdictional claims in published maps and institutional affiliations.

Springer Nature or its licensor (e.g. a society or other partner) holds exclusive rights to this article under a publishing agreement with the author(s) or other rightsholder(s); author self-archiving of the accepted manuscript version of this article is solely governed by the terms of such publishing agreement and applicable law.